THE ORIGINS OF MAGNETIC DOMAINS

IN TITANOMAGNETITES

by

Jun Ye

A dissertation submitted in partial fulfillment
of the requirements for the degree of

Doctor of Philosophy

University of Washington

1993

Approved by Ronald T. Merrill
(Chairperson of Supervisory Committee)

Program Authorized
to Offer Degree Geophysics Program

Date December 23, 1992

Doctoral Dissertation

In presenting this dissertation in partial fulfillment of the requirements for the Doctoral degree at the University of Washington, I agree that the Library shall make its copies freely available for inspection. I further agree that extensive copying of this dissertation is allowable only for scholarly purposes, consistent with "fair use" as prescribed in the U.S. Copyright Law. Requests for copying or reproduction of this dissertation may be referred to University Microfilms, 1490 Eisenhower Place, P.O. Box 975, Ann Arbor, MI 48106, or to the author.

Signature 

Date 2-20-98

University of Washington

Abstract

THE ORIGINS OF MAGNETIC DOMAINS IN TITANOMAGNETITES

by Jun Ye

Chairperson of the Supervisory Committee: Professor Ronald T. Merrill

Geophysics Program

The effects of macrostress on domain structures are investigated by using one dimensional models in laminar and closure domain structures. It is found that for Ti-rich titanomagnetite, domain structures are dependent on the magnitude and orientation of the stress. When the stress is small ($\sigma \ll 100 Bar$), the effects of macrostress is ignorable. When $\sigma \approx 100 Bar$, domain structures depend upon the orientation and the magnitude of the stress. The number of domains can be more or less than those for the zero stress state. When the stress is large ($\sigma \gg 100 Bar$), grains will have fewer number of domains than for the zero stress state and they will exhibit simple domain patterns. For Ti-rich titanomagnetite, there is an inconsistency between the number of domains predicted by theory and observed. It is shown that this can be explained by high stress (1000 Bar) within the grains. Almost the same value of stress is estimated to explain observed trans-domain processes in AMTM60. In contrast, it is shown that for Ti-poor titanomagnetite (e.g. magnetite), macrostress does not appear to have significant effects on domain structures.

External field, temperature, macrostress, defects, and the size and shape of a grain are important factors for transdomain processes. Whether interior or exterior denucleation occurs depends on the size and shape of a grain and the variations in the external magnetic field. For Ti-rich titanomagnetite, large macrostress can stabilize the distribution in the number of domains with varying temperature. For Ti-poor titanomagnetite, transdomain

processes are expected to be more common as temperature is changed than for Ti-rich titanomagnetite. It is shown that defects can have both short range (as recognized before) and long range effects on transdomain processes and domain wall movements in magnetic grains.

The lengths of dislocations pinning domain walls are estimated through numerically simulating observed transdomain processes. It is found that for Ti-rich titanomagnetite (e.g. AMTM60), domain walls can be effectively pinned by a single dislocation. In contrast, this seems unlikely in pure magnetite.

Renormalization group methods have been used to explained the wide range of local energy domain states observed for TRM in titanomagnetite. It is shown that this wide distribution cannot occur by classical transdomain processes. Instead, it appears to be associated with thermal fluctuations within a degree below titanomagnetite's Curie temperature. The theory predicts that domain imaging can be very useful in practice to distinguish primary TRM from some forms of secondary magnetizations (e.g. grain growth CRM), and can also be used to determined if significant transdomain processes have occurred which is important in appraising the quality of a sample in a paleomagnetic research.

TABLE OF CONTENTS

LIST OF FIGURES

LIST OF TABLES

LIST OF SYMBOLS

b	Bias rate
c_{11}, c_{12}, c_{44}	Elastic constants
d	Grid size
e_w	Wall energy per unit area
l	Dislocation length
p	Probability
w	Wall thickness
A	Exchange constant
D	Grain size
E_a	Magnetic anisotropy energy
E_{el}	Elastic energy
E_{ex}	Exchange energy
E_f	External field energy
E_k	Magnetocrystalline anisotropy energy
E_m	Magnetostatic energy
E_{mel}	Magnetoelastic energy
E_t	Total magnetic energy
E_w	Wall energy
E_λ	Magnetostriction energy
H_d	Demagnetizing field

H_{ex}	External magnetic field
K	Magnetocrystalline anisotropy constant
M_s	Saturation magnetization
N	Number of domains
S_w	Wall area
T	Temperature
T_c	Curie temperature
T_r	Room temperature
V	Volume
Ω	Partition function
α	Direction cosines of magnetization
λ	Magnetostriction constants
μ	Shear modulus
ρ	Bulk magnetic charge density
σ	Stress
σ_{ij}	Stress components
e_{ij}	Strain components
υ	Surface magnetic charge denisity

ACKNOWLEDGEMENTS

Most of all, I wish to express my sincere gratitude to my advisor, Professor Ronald T. Merrill, who introduced me to the research field of rock magnetism and provided patient guidance throughout my graduate studies at the University of Washington. I would also like to thank Professor Michael J. Brown for his editorial reading of the dissertation and for his comments that improved the final manuscript, Professor Paul H. Johnson for reading the dissertation, and Professor Robert L. Ingalls and John R. Booker for serving as my supervisory committee. I would give my special thanks to my wife, Yan Lin for her continuous support and taking care of our lovely daughter during the period of my study.

To My Parents and My Family

CHAPTER 1

INTRODUCTION

The fact that magnetic minerals in rocks carry stable magnetic remanence throughout much of geological time allows geophysicists to determine the paleomagnetic field - its direction and possibly its intensity. To understand the mechanism of how rocks acquire and retain stable remanence is the prime interest of rock magnetists and the focus of this thesis.

The magnetic properties of rocks depend on the domain states of grains in magnetic minerals. The foundations of remanent magnetization theory was developed by Neel (1949) based on the assumption that the carriers of remanent magnetization are single domain grains. Very large multi-domain (MD) grains, although containing more volume than that of fine particles, have been shown experimentally not to be carriers of stable remanence (e.g. O'Reilly, 1984).

However, small MD grains are often experimentally found to behave similar to SD grains. Those grains therefore were called pseudo-single-domain (PSD) grains (Stacey, 1962). Since PSD grains have larger volumes relative to SD grains, the behavior of PSD grains is very interesting to rock magnetists. Several mechanisms for PSD behaviors have been suggested. These include the spin pinning by dislocations (Verhoogen, 1959); the Barkhausen discreteness of domain walls (Stacey, 1963); surface domains pinned by surface anisotropy and defects (Stacey and Banerjee, 1974; Banerjee, 1977); domain wall movements (Dunlop, 1977). All those mechanisms are based on the belief that PSD grains contain multi-domain structures (although their behavior is similar with SD grains). However, in the last decade, it was found that some small MD grains have SD structures in some remanent states but have MD structures in other states (Halgedahl and Fuller, 1983). The interpretation of this phenomenon is the local energy minimum (LEM) states theory given

by Moon and Merrill (1985). According to the theory, there is a set of local minimum energy states as well as one absolute minimum energy (AEM) state for a grain. Since there are energy barriers between the LEM states, a grain can be at different LEM states in different times. For a small MD grain, SD can be one of its LEM states. Therefore it was suggested that the failure of domain wall nucleation is the controlling mechanism for the behavior of PSD grains (Halgedahl and Fuller, (1983); Moon (1985).

The domain structure and remanence problem is very complex. In particular, one needs to consider the following factors. (1) What are the effects of having different types of domain and domain walls? (2) What are the processes of domain nucleation and denucleation? (3) How do domain walls move? (4) What is the nature of the interactions of domain walls with defects? (5) What are the effects of thermal variation on domain structures? (6) What are the effects of a magnetic field and of applied stresses on domain structures? Because these factors are interrelated, the problem is complicated. A full discussion of all the above is far beyond the scope of this thesis. The main contents of this thesis are closely related to three questions mentioned above. The questions addressed are related to the effects of macrostresses on domain structures (chapter 3); to transdomain processes (chapter 4); and to the effects of thermal variation on domain structures (chapter 5).

1.1 The effects of Macrostress on Domain Structures

The domain Bitter pattern observation technique has been the most commonly used experimental method in rock magnetism to investigate domain structures in large grains (e.g. Soffel, 1971; Halgedahl, 1991). Other methods include the Kerr effect (e.g. Hoffmann, et al; (1987), and Lorentz microscopy (e.g. Smith, (1980); and Morgan and Smith, (1981); Heider and Hoffmann, (1992)). It is almost the rule rather than the exception that grains are observed to have fewer domains than their theoretical predicted number. Although grains

can be in their LEM states (Moon and Merrill, 1985), the domain numbers for a given size grain are usually distributed in the lower end section of the LEM states range, and some even exhibit fewer domains than allowed by present theory (e.g. Moon, 1991). There are at least three possible explanations for the inconsistency between the predicted and observed number of domains. They are (a): observational error, i.e. that the Bitter pattern observed on the grains surface does not accurately represent the number of domains present; (b): the surface structures may not be representative of the interior of the grain and (c): the theoretical calculations are inaccurate or(and) there is some fundamental misunderstanding of theoretical aspects of domain structures.

Although some domain walls could be miss-imaged by Bitter pattern technique (Newell, et al, 1993), the effect does not seem large enough to explain the discrepancy between prediction and observation since the same discrepancy is observed in domain imaging (instead of walls) by the magneto-optical Kerr effect (Worm, et al, 1991). Effects of the interaction between the colloid particles and surface structures are not significant in this last technique.

Some evidence indicates that the magnetic structures in the interior of grains may be different from the surface structures. For example closure domains, which are sometimes observed in magnetite (e.g. Heider, et al. 1988; Boyd, 1986; Boyd, et al., 1984), are certainly a kind of surface structure. In addition to closure domains, a thin layer may exist beneath the surface of the grains, which has a very different structures from that of interior, in order to decrease the magnetostatic energy (Ye and Merrill, 1991, see Appendix A). Both structures exist on the surface that is perpendicular to magnetization direction of the main domains. On the surface that is parallel to the main domains there seems to be no observational evidence or theoretical reason to have significant surface structures, because there are no bound magnetic poles on those surfaces.

Although the number of domains observed depends on the orientation of magnetization of the main domains with respect to the observation surface, one would expect to observe a large number of domains, at least when the observation surface is perpendicular to the magnetization. But the fact is that the number of domains observed is not close to the upper limit of LEM states; it appears that there is roughly one order magnitude difference between the number of domains observed and predicted (e.g. Moon, 1991, Worm, et al, 1991).

Could the fact that the observed distribution of number of domains is displaced toward the lower part of LEM states range calculated be explained by the failure of nucleation and(or) denucleation of domain walls? This seems improbable: denucleation should seldom happen because the activation energy between the LEM states are usually much higher than thermal fluctuation energy characterized by kT (k: Boltzmann constant and T: absolute temperature). This is discussed further in chapter 4, along with the conditions that must be satisfied to allow domain denucleation to occur. In addition, the predicted number of domains for AEM states is also much higher than that observed after AF demagnetized (Halgedahl, 1991). Finally, it is worth noticing that denucleation processes are seldomly observed.

In most previous theoretical considerations of domain structure, the magnetic energy includes only magnetostatic energy, magnetocrystalline energy, and exchange energy. The magnetoelastic energy, which includes the magnetostriction energy and elastic energy, was thought to be negligible relative to the other three energies. But this seems unlikely in some cases (e.g. Worm, et al, 1991). Defects within crystals (e.g. dislocations) generate strong local stresses and can affect domain wall pinning (e.g. Xu and Merrill, 1989). However there should be more domains in the crystal with microstress than that in a perfect stochiometric crystal since in the imperfect crystal, domain walls cannot move freely to

minimize the magnetostatic energy. Moreover once a domain wall forms in an imperfect crystal it is harder to denucleate if it is pinned by defects.

In addition to the stresses generated by defects, macrostress exists in crystals. The sources of macrostress may be internal, due to magnetostriction, or external in origin, i.e. transferred by the matrix that surrounds the crystal. The former can be caused by the magnetization itself while the latter can be introduced by thermal expansion, or by surface polishing. Macrostress will affect the domain states of the crystal through magnetoelastic energy. In chapter 3, I will show how macrostress affects the domain states by considering specific closure domain and laminar domain models. It will be shown that the inconsistency between theory and domain imaging results is primarily a result of the presence of macrostress.

1.2 Trans-Domain Processes

One of the major difficulties in creating a theory of remanent magnetization for multi-domain grains is that there are typically a set of LEM states for a given crystal under fixed conditions (Moon and Merrill, 1985). That is, a multi-domain grain can be in different states at different times. To determine the remanent moment of an ensemble of grains one needs to know not only what the LEM states are (including the number of domains, the remanent magnetization, and the energy of them), but also the transitional processes between them. The former is a static part of the problem and the latter is the dynamic part. Kittel (1949) calculated the magnetic energy for simple domain structures with the assumption of infinitely thin domain walls. In the last decade, more precise calculations have been done using computers to allow for finite wall thickness (e.g., Moon and Merrill, 1984; Enkin and Dunlop, 1987). Although most previous studies have focused on the static part of the problem, trans-domain processes have been considered in a few instances (e.g. Moon

and Merrill, 1985). Brown (1963) analyzed the process of reversing the direction of magnetization of a uniformly magnetized grain and found that the coercivity is much larger than observed (Brown's paradox). The cause of this inconsistency is that the initial magnetic structure is not perfectly uniform, as was assumed by Brown. A nonuniformly magnetized initial structure will result in a lower coercivity (Hartmann, 1987).

Moon and Merrill (1985) were the first to model transdomain processes. They assumed a domain wall nucleated at a boundary of a grain and calculated the activation energies between LEM states. We call this model the exterior nucleation (denucleation) model and it is discussed further in chapter 4.

Recently, changes in domain states with temperature have been observed (Halgedahl, 1991). When a titanomagnetite grain was cooled from near its Curie temperature to room temperature, domain wall denucleation was sometimes observed to occur. In the process of this denucleation, two adjacent domain walls met in the interior of the grain and collapsed to denucleate a domain. This observation, not predicted by theory, is referred to as interior denucleation.

In chapter 4, we will compare the energy barriers between domain states for both interior and exterior nucleation (denucleation) models. The effects of an external field, grain shape and temperature on trans-domain processes will be discussed there.

1.3 Application of Renormalization Group Methods to Domain Theory

It was observed that there is a much wider range of LEM states for TRM than that for AF demagnetized states (Halgedahl, 1991). This phenomenon cannot be explained by classical trans-domain processes. Renormalization group theory related to critical point phenomena will be used to explain the initial formation of domains in chapter 5. Some applications of this theory to paleomagnetism will also be discussed, including the

suggestion of methods to distinguish some forms of secondary magnetizations from primary magnetization.

CHAPTER 2

MAGNETIC ENERGIES IN DOMAINS AND DOMAIN WALLS

It is well known that domain structures are determined by minimizing the free energy. Therefore in order to investigate domain structures theoretically one needs to know the magnetic energies and their relationship to domain structures. This chapter briefly introduces the magnetic energies which determine the magnetic domain structures. More detailed discussions of the relevant magnetic energies can be found in Brown (1963), Chikazumi (1964), and Morrish (1965).

2.1 Magnetic Energies

For a magnetic material with finite volume, there are five kinds of magnetic energies. They are exchange energy (E_{ex}), magnetocrystalline energy (E_k), magnetoelastic energy (E_{mel}), magnetostatic energy (E_s), and external field energy (E_f). The total magnetic energy therefore equals:

$$E_t = E_{ex}+E_k+E_{mel}+E_s+E_f \tag{2.1}$$

2.1.1 Exchange energy

The exchange energy originates from the exchange interaction between the electron spins of neighboring atoms or ions. It can be expressed for a cubic crystal as

$$E_{ex} = A\int[(\nabla\alpha_1)^2+(\nabla\alpha_2)^2+(\nabla\alpha_3)^2]dv \tag{2.2}$$

where A is the exchange constant of the mineral and α_1, α_2 and α_3 are the direction cosines of magnetization. The integral is over the volume of the crystal.

2.1.2 Magnetocystalline Anisotropy Energy

With magnetic anisotropy, internal energy depends on the direction of spontaneous magnetization. Since the magnetic anisotropy energy term possesses the crystal symmetry of the material, it is defined as the magnetocrystalline anisotropy. Applying mechanical stress to a material produces magnetostrictive anisotropy. An external magnetic field can also introduce magnetic anisotropy though the interaction between the field and the magnetization of the material. The magnetic anisotropy produced by stress and external fields are discussed in the following sections.

Magnetocrystalline anisotropy primarily originates from spin-orbit coupling. Magnetocrystalline energy E_k for uniaxial anisotropy crystal is

$$E_k = K_u \int \sin^2\theta dv \tag{2.3}$$

with θ being the angle between magnetization and the easy direction of the crystal. For a cubic crystal E_k can be written in a first order approximation as

$$E_k = K_1 \int (\alpha_1^2\alpha_2^2+\alpha_2^2\alpha_3^2+\alpha_3^2\alpha_1^2) dv \tag{2.4}$$

with K_1 being the magnetocrystalline constant and α_1, α_2 and α_3 are the direction cosines of magnetization with respect to [100], [010] and [001] axes of the crystal respectively. For crystals with $K_1>0$, the easiest directions are [100], [010] and [001] directions, while the hardest directions are [111], [$\bar{1}$11], [$\bar{1}\bar{1}$1], and [1$\bar{1}$1]. For $K_1<0$, the easy directions become [111], [$\bar{1}$11] , [$\bar{1}\bar{1}$1], and [1$\bar{1}$1] while the hardest directions become [100], [010] and [001] as for the cases of magnetite and titanomagnetite.

2.1.3 Magnetoelastic Energy

Magnetoelastic energy, E_{mel}, originates in the interaction between the atomic magnetic moments. It is different from magnetocrystalline anisotropy energy in that the

magnetoelastic energy is related to the deformation of the lattice. Therefore magnetoelastic energy includes two parts: magnetostriction energy (E_λ) and elastic energy (E_{el}). The magnetostriction energy can be expressed as

$$E_\lambda = -\frac{3}{2}\lambda_{100}\int(\sigma_{11}\alpha_1^2+\sigma_{22}\alpha_2^2+\sigma_{33}\alpha_3^2)dv \; -3\lambda_{111}\int(\sigma_{12}\alpha_1\alpha_2+\sigma_{23}\alpha_2\alpha_3+\sigma_{13}\alpha_3\alpha_1)dv \qquad (2.5)$$

Where λ_{100} and λ_{111} are the magnetostriction constants along [100] and [111] respectively and σ_{ij} are the components of a stress tensor. The elastic energy for cubic crystal (e.g. magnetite and titanomagnetite) is

$$E_{el} = \int[\frac{1}{2}c_{11}(e_{11}^2+e_{22}^2+e_{33}^2)+\frac{1}{2}c_{44}(e_{12}^2+e_{23}^2+e_{13}^2)+c_{12}(e_{11}e_{22}+e_{22}e_{33}+e_{11}e_{33})]dv \qquad (2.6)$$

Where c_{11}, c_{44} and c_{44} are the elastic constants and e_{ij} is strain tensor.

The magnetoelastic energy ($E_{mel} = E_\lambda+E_{el}$) depends on whether the crystal is in the magnetostriction state or the inverse magnetostriction state. The magnetostriction state is defined as state in which the stress within the crystal is generated by the magnetostriction effect itself. This stress can be determined by minimizing magnetoelastic energy with respect to stress. That is, by using

$$\frac{\partial E_{mel}}{\partial \sigma_{ij}}=0 \qquad i,j=1,2,3 \qquad (2.7)$$

and the relationship between strain and stress we can get the stress with minimum magnetoelastic energy, which is

$$\sigma_{ii} = \frac{3}{2}(c_{11}-c_{12})\lambda_{100}[\alpha_i^2-\frac{1}{3}] \qquad (i=1,2,3) \qquad (2.8)$$

and

$$\sigma_{ij} = 3c_{44}\lambda_{111}\alpha_i\alpha_j \qquad (i\neq j) \qquad (2.9)$$

Substitute (2.8) and (2.9) into (2.5) and (2.6), we get

$$E_{mel} = E_{\lambda}+E_{el} = -\frac{3}{4}(c_{11}-c_{12})\lambda_{100}^2+\frac{9}{4}[(c_{11}-c_{12})\lambda_{100}^2-2c_{44}\lambda_{111}^2](\alpha_1^2\alpha_2^2+\alpha_2^2\alpha_3^2+\alpha_1^2\alpha_3^2) \quad (2.10)$$

The first term on the right hand side of (2.10) is a constant which does not depend on the direction of magnetization. The second term has a same dependence on α_1, α_2 and α_3 as the magnetocrystalline energy. Therefore the effect of magnetostriction is simply to replace K_1 in (2.4) by an effective anisotropy constant, K_1', given by

$$K_1' = K_1+\frac{9}{4}[(c_{11}-c_{12})\lambda_{100}^2-2c_{44}\lambda_{111}^2] \quad (2.11)$$

When a crystal is subjected to stress generated by its surroundings or by internal defects, the crystal is in an inverse magnetostriction state. In this case, the stresses subjected by the lattice not only originate from the magnetostriction effect, but also from the mechanical sources (e.g. defects). Therefore there is extra magnetoelastic energy which includes the magnetostriction energy and the elastic energy caused by the mechanical stress. These are given in (2.5) and (2.6) respectively. The total magnetocrystalline anisotropy energy and magnetoelastic energy is given by the summation of (2.4) (with K_1 replaced by K_1'), (2.5) and (2.6). However, for inverse magnetostriction case, the elastic energy generated by the mechanical stress (2.6) is not related with the magnetic structure of the crystal. Therefore one does not need to consider it when the interest is only in magnetic domain structures.

2.1.4 Magnetostatic Energy

Magnetostatic energy E_s, or the demagnetization energy, originates from the interactions between magnetic moments in the material and can be expressed in terms of the demagnetizing field, $\vec{H}_d$:

$$E_s = -\frac{1}{2}\int \vec{H}_d \cdot \vec{M}_s \, dv \tag{2.12}$$

The demagnetizing field, $\vec{H}_d$, at a point $\vec{r}$ is

$$\vec{H}_d = -\frac{1}{2}\nabla \int_{V'} \frac{\rho'}{|\vec{r}-\vec{r}'|} dv' - \nabla \int_{S'} \frac{\upsilon'}{|\vec{r}-\vec{r}'|} ds' \tag{2.13}$$

Therefore the magnetostatic energy is

$$E_s = \frac{1}{2}\iint_{VV} \frac{\rho\rho'}{|\vec{r}-\vec{r}'|} dv dv' + \iint_{SV} \frac{\upsilon\rho'}{|\vec{r}-\vec{r}'|} ds dv' + \frac{1}{2}\iint_{SS} \frac{\upsilon\upsilon'}{|\vec{r}-\vec{r}'|} ds ds' \tag{2.14}$$

where $\rho=-\nabla\cdot\vec{M}_s(x,y,z)$ and $\rho'=-\nabla'\cdot\vec{M}_s(x',y',z')$ are the volume charge densities, $\upsilon=\vec{n}\cdot\vec{M}_s(x,y,z)$ and $\upsilon'=\vec{n}\cdot\vec{M}_s(x',y',z')$ are the surface densities with $\vec{n}$ being the unit vector of the normal of the surface. $\vec{M}_s$ is the saturation magnetization. $\vec{r}=\vec{r}(x,y,z)$ and $\vec{r}'=\vec{r}'(x',y',z')$ are the positions of integral elements. It is important to mention that because the integral limits in (2.12) and (2.13) are same, they are not distinguished in (2.14); they are the volume of the grain, V, and the surface of the grain, S.

2.1.5 External field energy

The external field energy E_f can be expressed as

$$E_f = -\int \vec{H}_{ex} \cdot \vec{M}_s \, dv = -\vec{H}_{ex} \cdot \vec{M} \tag{2.15}$$

Where $\vec{H}_{ex}$ is the external field. With the condition of $\vec{H}_{ex}$ being constant within the whole crystal, the second equality is valid, with the magnetic moment of the grain given by $\vec{M} = \int \vec{M}_s \, dv$.

2.2 Anisotropy Energy in Domains and Domain Wall Energy

In this section, we will calculate the energies of domains and domain walls by using the equations given above.

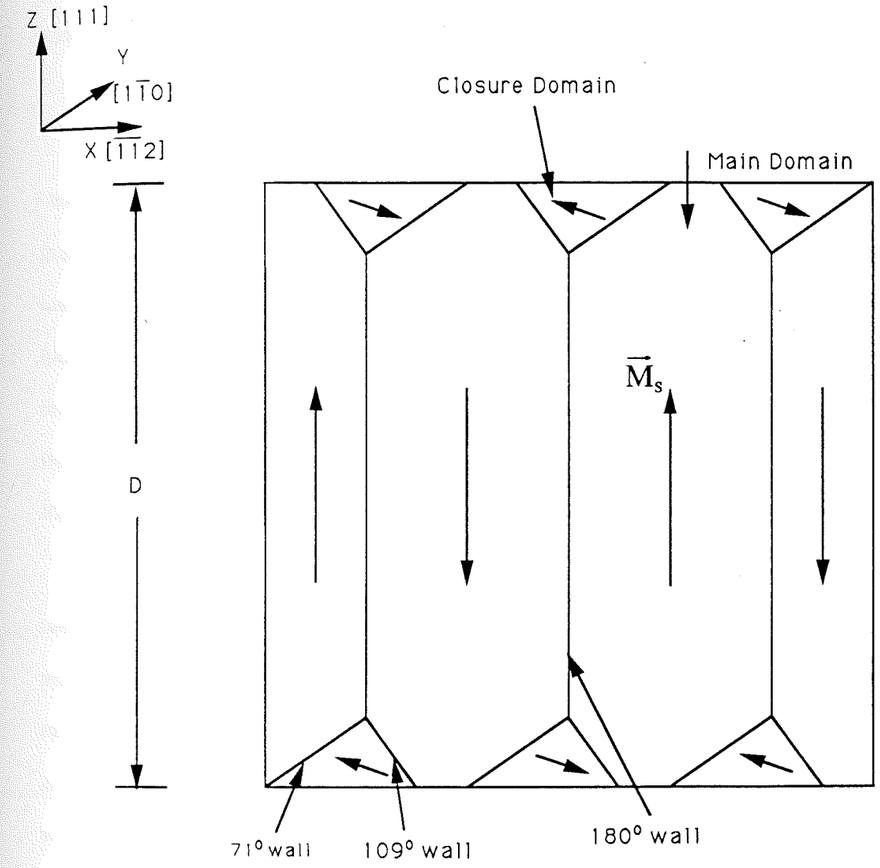

Figure 2.1 A cubic grain with closure domain structure. Both main domains and closure domains are present. The arrows in each domain gives the direction of magnetization.

First we introduce the coordinate system. For magnetite and titanomagnetite, K_1' is less than zero, thus the [111] directions are easy directions of magnetization. For a grain as shown in figure 2.1, we assume $\vec{Z}$ along [111], X along $[\bar{1}\bar{1}2]$, and $\vec{Y}$ along $[1\bar{1}0]$ (figure 2.1).

The are two kinds of domains, the main domains and the closure domains, in the grain shown in figure 2.1. The main domains are those domains occupy the most volume of the grain. Since the direction of magnetization in main domains is along ±[111] directions, the main domains have the lowest magnetic anisotropy energy. The closure domains, which are located at the surface of the grain, reduce the magnetostatic energy of the crystal. The directions of magnetization in closure domains are taken to be along the $\pm[11\bar{1}]$ directions. Between the domains, there are three kinds of domain walls. They are 180°, 71° and 109° Bloch walls.

We consider the anisotropy energies of domains and domain wall in two different cases: the magnetostriction case and the inverse magnetostriction case. For the inverse magnetostriction case, magnetoelastic energy depends on the stress tensor (2.5). For simplicity sake, the energies with only one simple stress state (uniaxial compression or extension along [111]) will be calculated in this section. The effects of general stresses on domain structures is discussed in next chapter. The stress tensor for an uniaxial stress along [111] is

$$\sigma_{ij} = \frac{T_{111}}{3}\begin{bmatrix} 1 & 1 & 1 \\ 1 & 1 & 1 \\ 1 & 1 & 1 \end{bmatrix} \tag{2.16}$$

Here T_{111} is the magnitude of the uniaxial stress.

2.2.1 The energy of domains

For main domains, the magnetization is along ±[111] directions. For the magnetostriction case, the anisotropy energy density is (2.4).

We begin our wall energy discussion by briefly reviewing classical domain wall theory (e.g. Chikazumi, 1964). The assumption in determining the structure of a Bloch wall is that the wall does not possess any volume magnetic bound poles, i.e. $\nabla\cdot\vec{M}_s=0$, where M_s is the saturation magnetization. This condition requires that the angle between the magnetization and the normal to the wall plane is a constant for the whole wall.

The 180°, 71° and 109° Bloch walls can exist in cubic crystals with $K_1<0$ if there is no external macrostress. The angles between the magnetization and the normal to the wall plane therefore are 90°, 35.5° and 54.5° respectively for the above three kinds of walls (figure 2.2). In this case, the domain wall energy, e_w, per unit area consists only of the exchange and magnetic anisotropy energies, i.e.

$$e_w = \int\left[A\sin^2\theta(d\phi/dx)^2+e_a\right]dx \tag{2.21}$$

where A is the exchange constant, θ is the angle between the magnetization direction and the normal of the wall plane. e_a is the density of the anisotropy energy with respect to the anisotropy energy of domain beside the wall. It follows from a variational treatment that, for e_w to have a minimum value, the exchange and anisotropy contributions to the energy must be equal(Lilley, 1950). Therefore the variation of the direction of magnetization can be determined by

$$(dx/d\phi)= A^{1/2}\sin\theta e_a^{-1/2} \tag{2.22}$$

And the wall energy therefore is

$$e_w = \int 2e_a dx = \int 2e_a(dx/d\phi)d\phi = 2A^{1/2}\sin\theta\int_{\phi_1}^{\phi_2} e_a^{1/2}d\phi \tag{2.23}$$

Where ϕ is the azimuth angle of magnetization, and ϕ_1 and ϕ_2 are ϕ values of the two domains adjacent to the wall (for details, see Lilley, 1950).

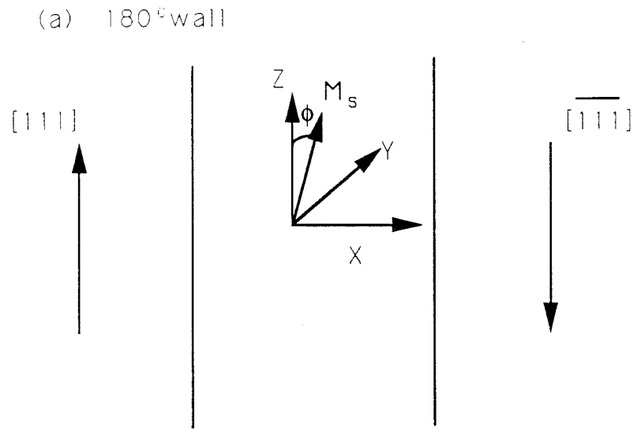

Figure 2.2 The magnetization vector rotation mode for (a) 180°; (b) 71° and (c) 109° Bloch walls. For 180° wall, the magnetization is in Y–Z plane. For 71° and 109° walls, magnetization vector stays on the cones with a constant θ in (b) and (c).

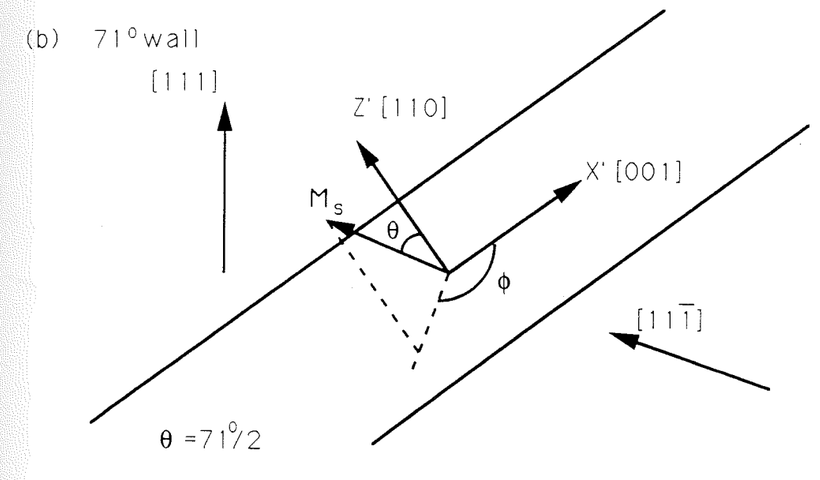

Figure 2.2 Continued.

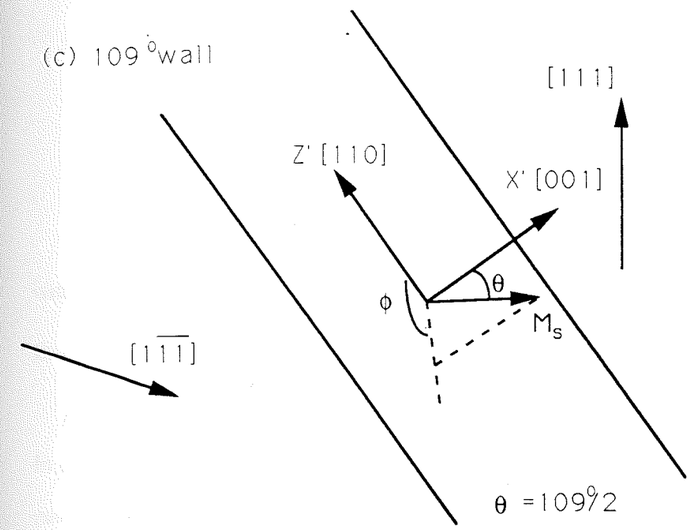

Figure 2.2 Continued.

$$e_{w180^\circ} = 2.0040\times(A\,|K_1'|)^{1/2}\approx 2(A\,|K_1'|)^{1/2} \tag{2.28}$$

For inverse magnetostriction case, substitute (2.26) into (2.4) and (2.5) and subtract (2.18). Then we get the anisotropy energy density at $\phi(x)$:

$$e_a = K_1'\left[\frac{1}{3}\cos^4\phi+\frac{1}{4}\sin^4\phi-\frac{1}{3}\right]+\frac{9}{2}\sigma_{12}\lambda_{111}\sin^2\phi \tag{2.29}$$

And the wall energy therefore becomes

$$e_{w180^\circ} = [A\,|K_1'|[(1+\tau)/3]^{1/2}[(\varepsilon+1)^{1/2}+\varepsilon^{-1/2}\sinh^{-1}(\varepsilon^{1/2})] \tag{2.30}$$

with $\varepsilon = 7/(1+\tau)$, and $\tau = 54\sigma_{12}\lambda_{111}/|K_1'|$ (for details, see Lilley, 1950).

Energies for 71° and 109° walls

For 71° wall, the magnetization changes from [111] to [11$\bar{1}$] in the wall (figure 2.2b). In order to derive the equations of wall energy, it is convenient to introduce another coordinate system denoted as $X'Y'Z'$. As shown in figure 2.2b, X' axis is along [001], Y' along [1$\bar{1}$0] and Z' along [110]. The direction cosines of the magnetization at ϕ with respect to $X'Y'Z'$ system are

$$\alpha_{x'} = \sin\theta\cos\phi$$

$$\alpha_{y'} = \sin\theta\sin\phi \tag{2.31}$$

$$\alpha_{z'} = \cos\theta$$

with θ equals $\frac{71^\circ}{2}$. The transformation matrix between the $X'Y'Z'$ system and [100], [010], [001] system is

$$\begin{pmatrix} \alpha_{1x'} & \alpha_{1y'} & \alpha_{1z'} \\ \alpha_{2x'} & \alpha_{2y'} & \alpha_{2z'} \\ \alpha_{3x'} & \alpha_{3y'} & \alpha_{3z'} \end{pmatrix} = \begin{pmatrix} 0 & \frac{\sqrt{2}}{2} & \frac{\sqrt{2}}{2} \\ 0 & -\frac{\sqrt{2}}{2} & \frac{\sqrt{2}}{2} \\ 1 & 0 & 0 \end{pmatrix} \tag{2.32}$$

So we get the direction cosines of $\vec{M}_s$ with respect to [100], [010] and [001] as

$$\alpha_1 = \frac{\sqrt{2}}{2}(cos\,\theta + sin\,\theta\sin\phi)$$

$$\alpha_2 = \frac{\sqrt{2}}{2}(cos\,\theta - sin\,\theta\sin\phi) \tag{2.33}$$

$$\alpha_3 = \sin\theta\cos\phi$$

By using a similar derivation as used in 180° wall case, we get the wall energy per unit area for 71° wall in both the magnetostriction case and the inverse magnetostriction case.

For the magnetostriction case, by using (2.33), (2.4), (2.17), and (2.23) the energy of 71° wall is given by

$$e_{w71^\circ} = 2A^{1/2}\sin\theta \int_{0^\circ}^{180^\circ} \Big[K_1'[\sin^2\theta\cos^2\theta\cos^2\phi + sin^4\theta\cos^2\phi\sin^2\phi + \frac{1}{4}\cos^4\theta + \frac{1}{4}\sin^4\theta\sin^4\phi \tag{2.34}$$

$$-\frac{1}{2}\cos^2\theta\sin^2\theta\sin^2\phi - \frac{1}{3}] \Big]^{1/2} d\phi$$

Since $\theta = \frac{71^\circ}{2}$, $\sin^2\theta = \frac{1}{3}$, $\cos^2\theta = \frac{2}{3}$, we get

$$e_{w71^\circ} = \frac{2}{3\sqrt{3}} A^{1/2} \int_{0^\circ}^{180^\circ} \Big[K_1'(2cos^2\phi + cos^2\phi\sin^2\phi + \frac{1}{4}\sin^4\phi - sin^2\phi - 2) \Big]^{1/2} d\phi \tag{2.35}$$

By using (2.33), (2.4), (2.5), (2.18) and (2.23), we get the 71° wall energy for the inverse magnetostriction case as

$$e_{w71^\circ}=2A^{1/2}\sin\theta\int_{0^\circ}^{180^\circ}\Big[K_1'[\sin^2\theta\cos^2\theta\cos^2\phi+sin^4\theta\cos^2\phi\sin^2\phi+\frac{1}{4}\cos^4\theta+\frac{1}{4}\sin^4\theta\sin^4\phi \tag{2.36}$$

$$-\frac{1}{2}\cos^2\theta\sin^2\theta\sin^2\phi-\frac{1}{3}]-3\lambda_{111}\sigma_{12}[\sqrt{2}\sin\theta\cos\theta\cos\phi+\frac{1}{2}(cos^2\theta-\sin^2\theta\sin^2\phi)-1]\Big]^{1/2}d\phi$$

With $\theta = \frac{71^\circ}{2}$, $\sin^2\theta = \frac{1}{3}$, $\cos^2\theta = \frac{2}{3}$, we get

$$e_{w71^\circ} = \frac{2}{\sqrt{3}}A^{1/2}\int_{0^\circ}^{180^\circ}\Big[\frac{K_1'}{9}(2cos^2\phi+cos^2\phi\sin^2\phi+\frac{1}{4}\sin^4\phi-sin^2\phi-2) \tag{2.37}$$

$$-\lambda_{111}\sigma_{12}(2cos\,\phi-\frac{1}{2}\sin^2\phi-2)\Big]^{1/2}d\phi$$

For a 109° wall, the directions at the sides of the wall are [111] and $[\overline{1}11]$ (figure 2.2c). The direction cosines of the magnetization in the wall in $X'Y'Z'$ coordinate system are

$$\alpha_{x'} = \cos\theta$$

$$\alpha_{y'} = \sin\theta\sin\phi \tag{2.38}$$

$$\alpha_{z'} = \sin\theta\cos\phi$$

with $\theta = \frac{109^\circ}{2}$ and ϕ from 0° to 180°. Using (2.32), the direction cosines in [100], [010] and [001] system are given by

$$\alpha_1 = \frac{\sqrt{2}}{2}\sin\theta(cos\,\phi+sin\,\phi)$$

$$\alpha_2 = \frac{\sqrt{2}}{2}\sin\theta(cos\,\phi-sin\,\phi) \tag{2.39}$$

$$\alpha_3 = \cos\theta$$

Following the same procedure as for 180° wall, we then get the energy for 109° wall in magnetostriction case as

$$e_{w\,109^\circ} = 2A^{1/2}\sin\theta \int_{0^\circ}^{180^\circ}\left[K_1'(\cos^2\theta\sin^2\theta+\frac{1}{4}\sin^4\theta(cos^2\phi-sin^2\phi)^2-\frac{1}{3}]\right]^{1/2} d\phi \qquad (2.40)$$

Since for 109° wall $\theta = \frac{109^\circ}{2}$, $\sin^2\theta = \frac{2}{3}$, $\cos^2\phi = \frac{1}{3}$, we get

$$e_{w\,109^\circ} = \sqrt{\frac{8}{27}}A^{1/2}\int_{0^\circ}^{180^\circ}\left[K_1'[(\cos^2\phi-\sin^2\phi)^2-1]\right]^{1/2} d\phi \qquad (2.41)$$

While for inverse magnetostriction case, we have

$$e_{w\,109^\circ} = 2A^{1/2}\sin\theta \int_{0^\circ}^{180^\circ}\left[K_1'(\cos^2\theta\sin^2\theta+\frac{1}{4}\sin^4\theta(cos^2\phi-sin^2\phi)^2-\frac{1}{3}] \qquad (2.42)$$

$$-3\lambda_{111}\sigma_{12}[\sqrt{2}\sin\theta\cos\theta\cos\phi+\frac{1}{2}\sin^2\theta(cos^2-sin^2\phi)-1]\right]^{1/2} d\phi$$

with $\theta = \frac{109^\circ}{2}$, $\sin^2\theta = \frac{2}{3}$,$\cos^2\phi = \frac{1}{3}$, we get

$$e_{w\,109^\circ} = \sqrt{\frac{8}{3}}A^{1/2}\int_{0^\circ}^{180^\circ}\left[\frac{K_1'}{9}[(\cos^2\phi-\sin^2\phi)^2-1]-\lambda_{111}\sigma_{12}(cos^2\phi-sin^2\phi+2cos\,\phi-3)\right]^{1/2} d\phi \qquad (2.43)$$

CHAPTER 3

EFFECTS OF MACROSTRESSES ON DOMAIN STRUCTURES

By macrostress, we mean that the stress has a much longer wave length for its spatial variation than the crystal size being considered. Therefore stress is uniform throughout the whole crystal. Without macrostresses, the closure domain pattern is usually the lowest energy state since closure domains on the grain surface effectively reduce the magnetostatic energy of the crystal. But if a crystal is subject to macrostresses, the energy of closure domains and the energy of domain walls will change with the stress. In this chapter, we investigate the domain structure variation with the magnitude of macrostresses though energy calculations for closure domain state and laminar domain state for magnetite and Ti-rich titanomagnetite ($Ti_{0.56}Fe_{2.44}O_4$, also referred as TM56). Also we show that high magnitude macrostresses cause far fewer domains in a given size crystal than that predicted by theory that neglects stress. In section 3.4, we estimate the magnitude of macrostresses for an Aluminium-magnesium Ti-rich titanomagnetite ($Al_{0.1}Mg_{0.1}Ti_{0.6}Fe_{2.2}O_4$) grain in which trans-domain processes have been observed.

3.1 The Model

3.1.1 Domain Structure

Consider a magnetic crystal (e.g., magnetite or titanomagnetite) with a cubic shape and linear size D. The domain structures are assumed to be two dimensional with N main domains and $2(N-1)$ closure domains (figure 3.1). The magnetizations in main domains are along $\pm[111]$ axes of the crystal while in closure domains the magnetizations are along $\pm[11\bar{1}]$ directions and separated by 71° and 109° Bloch walls from the main domains.

For simplicity sake, it is assumed that domain walls are infinite thin (more discussion

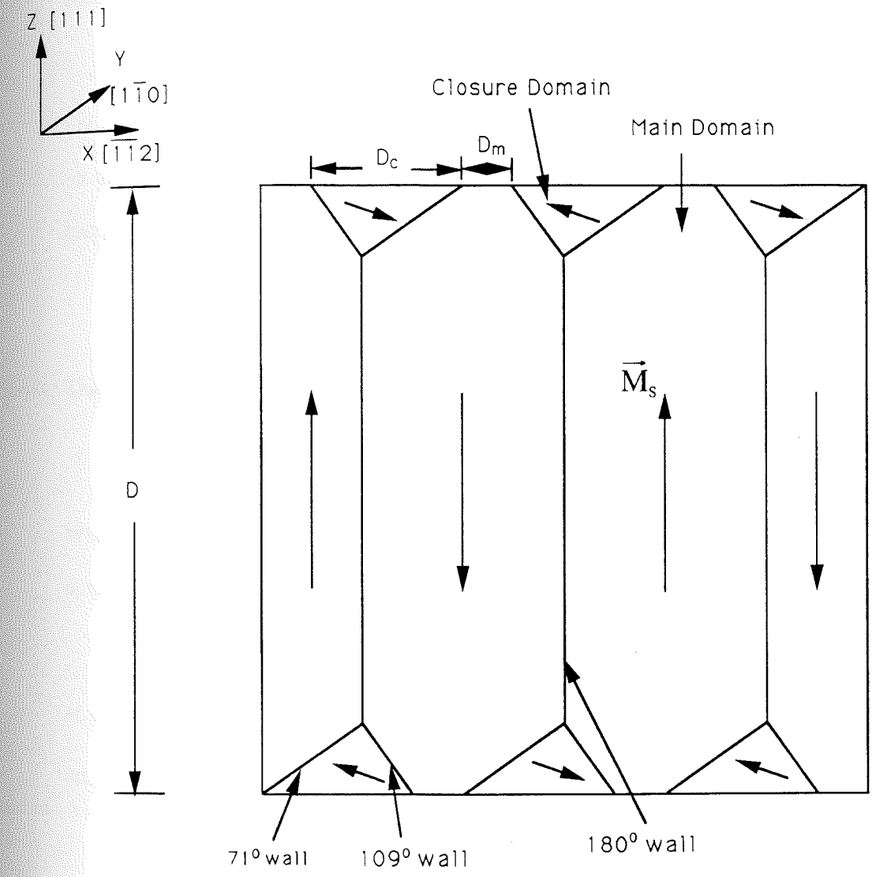

Figure 3.1 The closure domain model. D_c and D_m are the closure domain width and the main domain domain width.

about this assumption will be given in the next section). If we denote the widths of the main and closure domains on $X-Y$ surface as D_m and D_c respectively, we have

$$D = (N-1)(D_m+D_c) \tag{3.1}$$

Let us define parameter η being the percent of surface area covered by the closure domains on the $X-Y$ plane. η as an indicator of the size of closure domains will be determined by an energy minimization process. With the infinitely thin wall assumption, η is given by

$$\eta \equiv \frac{D_c}{D_m+D_c} \tag{3.2}$$

This gives

$$D_m = \frac{(1-\eta)}{(N-1)}D \quad \text{and} \quad D_c = \frac{\eta}{(N-1)}D \tag{3.3}$$

When η=1, the closure domains cover the whole surface of the grain; when η=0, no closure domains exist and the grain has a laminar domain structure.

The magnetic charge pole densities at the surface of the closure domains are $M_s\cos 71° = \frac{M_s}{3}$ and $M_s\cos 109° = -\frac{M_s}{3}$. While the densities on the surface of main domains are $\pm M_s$.

It is easy to get the volume of the closure domains (V_{cd}) and the areas of 180°, 71° and 109° walls from the geometry in figure 3.1. They are

$$V_{cd} = \frac{1}{2}\frac{\eta^2}{(N-1)}\sin(71°)D^3$$

$$A_{w\,180°} = [N-1-\eta\sin(71°)]D^2 \tag{3.4}$$

$$A_{w\,71°} = 2\eta\cos\left[\frac{71°}{2}\right]D^2$$

$$A_{w109^\circ} = 2\eta \sin\left[\frac{71^\circ}{2}\right] D^2$$

3.1.2 Infinitely Thin Wall Assumption

For uniaxial anisotropy crystal, the width of 180° Bloch wall is given by (e.g., Chikazumi, 1964)

$$w = \pi\left[\frac{A}{K_u}\right]^{1/2} \tag{3.5}$$

Here K_u is uniaxial magnetocrystalline anisotropy constant.

For cubic crystal, the wall width can be expressed by (3.5) approximately by using an equivalent unaxial magnetocrystalline constant given by:

$$K_u = -K'_1 \tag{3.6}$$

for the magnetostriction case and

$$K_u = -K'_1 + \frac{9}{2}\sigma_{12}\lambda_{111} \tag{3.7}$$

for the inverse magnetostriction case with the stress tensor given by (2.16).

By using (3.5) and (3.6) for magnetite and TM56 (constants given in table 3.1), we get the wall widths as $0.09\mu m$ and $0.07\mu m$ respectively for the magnetostriction case. Because w is much smaller than the domain sizes (a few microns) considered in this thesis, we ignore the wall width when we calculate the magnetostatic energy, i.e., we assume that the domain walls are infinitely thin. Of course, we still obtain the total wall energy with finite width walls (see chapter 2).

For the inverse magnetostriction case, the value of K_u depends on the stress σ_{12}. In the majority of this chapter, we assume $\sigma_{12}>0$, i.e., the stress is an extensional stress. When

Table 3.1 The magnetic variables for magnetite and TM56 at room temperature (T_r=300°K) and at 1 atm.

Variable	Magnetite	TM56	References
M_s	$480\times10^3 A/m$	$139\times10^3 A/m$	(1),(3)
A	$1.17\times10^{-11} J/m$	$0.31\times10^{-11} J/m$	(1)
K_1'	$-1.36\times10^4 J/m^3$	$-0.70\times10^4 J/m^3$	(2)
λ_{111}	78×10^{-6}	92×10^{-6}	(2)
λ_{100}	-19×10^{-6}	170×10^{-6}	(2)
c_{44}	$9.7\times10^{10} N/m^2$	$6.5\times10^{10} N/m^2$	(3)

References are (1), Moskowitz and Halgedahl (1987); (2) Syono (1965) and (3) Carmichael (1982)

$\sigma_{12}>0$, one gets a larger K_u for the inverse magnetostriction case (3.7) relative to the magnetostriction case (3.6). Therefore the wall width for the inverse magnetostriction case is smaller than that for the magnetostriction case and infinitely thin wall assumption is still valid. The effects of more general stresses (including the case for $\sigma_{12}<0$) will be discussed briefly in section 3.3.

3.1.3 Magnetic Energies

By using the infinitely thin wall assumption, all the magnetic charge poles are located at the two x-y surfaces of the grain (figure 3.1). The magnetic pole density is $\pm M_s$ on the domain surfaces and $\pm\frac{M_s}{3}$ on the surfaces of closure domains. Rhodes and Rowlands (1954) have developed a method which can be used to calculate the magnetostatic energy in our model. The magnetostatic energy is

$$E_s = f(N,\eta)M_s^2 D^3 \tag{3.8}$$

with $f(N,\eta)$ being a function of number of domains (N) and the parameter η. η is defined as the amount of coverage of closure domains on the grain surface. $f(N,\eta)$ can be numerically calculated by using the methods given by Rhodes and Rowlands (1954).

The total magnetic energy is the summation of closure domain energy, domain wall energy, and magnetostatic energy and can be expressed as

$$E_t = E_s + e_{cd}V_{cd} + e_{w180^\circ}A_{w180^\circ} + e_{w71^\circ}A_{w71^\circ} + e_{w109^\circ}A_{w109^\circ} \tag{3.9}$$

The volume of the closure domains and the area of the domain walls are given by (3.4). For the magnetostriction case, the values of e_{cd}, e_{w180°, e_{w71° and e_{w109° are given by (2.19), (2.28), (2.35) and (2.41) respectively. For inverse magnetostriction case, they were given by (2.20), (2.30), (2.37) and (2.43).

For a given value σ_{12} (being zero for magnetostriction case) we can get the domain structure characterized by N and η by minimizing the total magnetic energy (3.9). The variation of N and η with the stress magnitude provide us with the information on the effects of macrostress on domain structures.

3.2 The Macrostress Effects on Domain Structure for a Specific Stress State

We will mainly consider the stress effects for TM56 (titanomagnetite $Ti_{0.56}Fe_{2.44}O_4$). Using magnetic constants for TM56 given in table 3.1, the reduced total magnetic energy, $\frac{E_t}{J_s^2 D^3}$, is calculated for different σ_{12} (0 to $100MPa$), N (1 to 60), η (0 to 1) and D (1 to $200\mu m$). For a given D and σ_{12}, N and η are determined by minimumizing the reduced total energy. In this section, we investigate the effects of the stress on the number of domains (N) and on the domain pattern (characterized by η).

3.2.1 Domain pattern changes with stress

Because the magnetostriction anisotropy energy within closure domains is proportional to the magnitude of stress (σ_{12}) (2.20) , larger stress reduces the volume of the closure domains. Figure 3.2 is an example for a 20 micron grain. It shows that when $\sigma_{12} = 0$, $\eta = 1$. This means that the total covered closure domain structures is energetical favored. In contrast, when $\sigma_{12} = 90MPa$, $\eta = 0$, i.e. there are no closure domains and the laminar domain structure is energetically favored. Although the existence of closure domains can reduce magnetostatic energy, it causes more magnetic anisotropy as well. As a result, the volume of closure domains is the largest (η=1) for the magnetostriction case and decreases with increasing stress. Domain pattern, therefore, changes from fully closure domain pattern to a more "laminar-like" pattern.

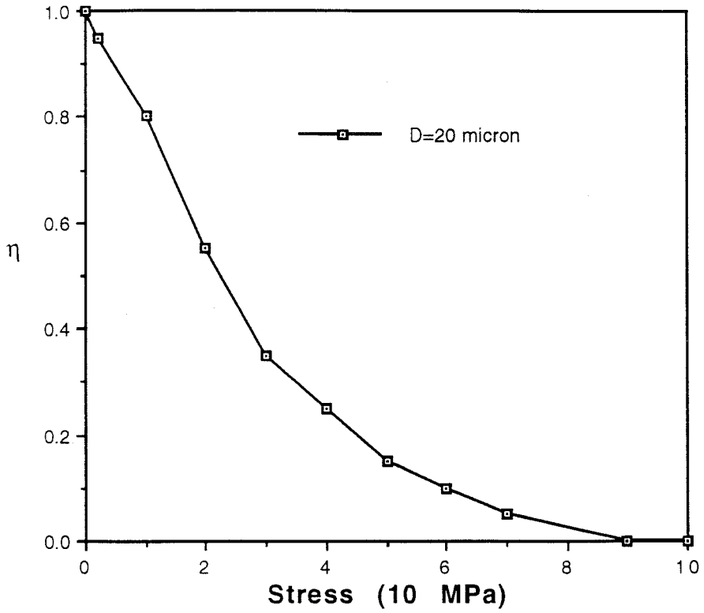

Figure 3.2 The variation of η with stress for D=20μm grain.

3.2.2 Changes in the number of domains with stress

For a given size grain, not only the domain pattern but also the number of domains are affected by macrostresses. As an example shown in figure 3.3 for a 20 micron grain, the number of domains of AEM states depends on the magnitude of the stress. When the external stress is small(less than $20MPa$), the number of domains increases with stress increasing. In contrast, when the stress ls large, the number of domains decreases with stress increasing. This phenomena can be qualitatively explained as follows. The volume of closure domains decreases with stress increasing as discussed in section 3.2.1. This would cause more magnetostatic energy. Consequently, when the stress is small, there will be more domains (and domain walls) within the grain (to reduce the magnetostatic energy). But when the stress is large, a state with fewer domains will be energetically favored since domain wall energy (per wall area) increases with stress. Consequently, depending on the stress state, a grain could have more or fewer number of domains than that for the zero external stress state.

3.2.3 Comparing Theory to Observed Data

The data points shown in figure 3.4 are the number of domains observed for titanomagnetite (TM55) at various grain sizes (Soffel, 1971). The three curves in figure 3.4 are theoretical results. They are: 1) the AEM state for laminar domain structures for the zero external stress case; 2) the AEM states for closure domain structure (η=1) with no external stress; and (3) the AEM states for a large externally applied stress ($\sigma_{12} = 100MPa$).

In the case of no external stress, the predicted number of laminar domains for AEM states is much greater than observed. However, as discussed in the last section , closure domain structures are energetically favored for small stress. Nevertheless, even the closure domain structure model is inadequate as shown.

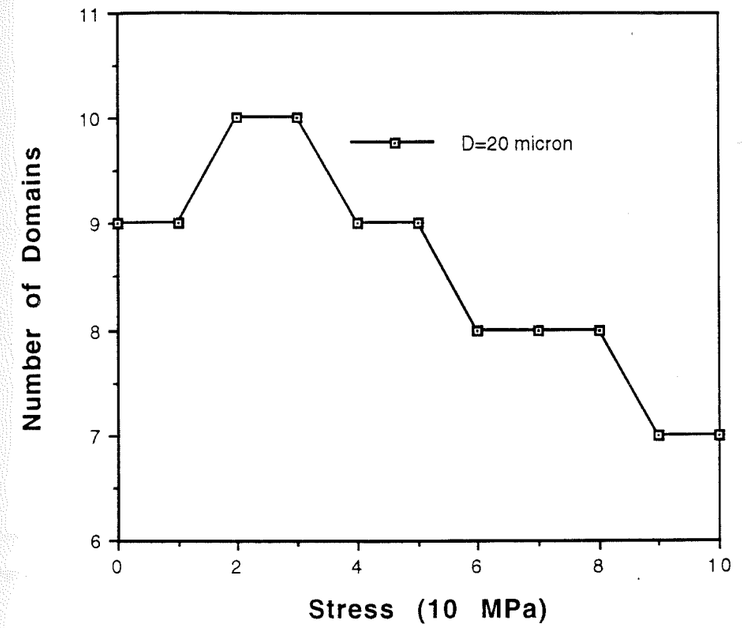

Figure 3.3 The number of domains for AEM states changes with stress for D=20μm grain.

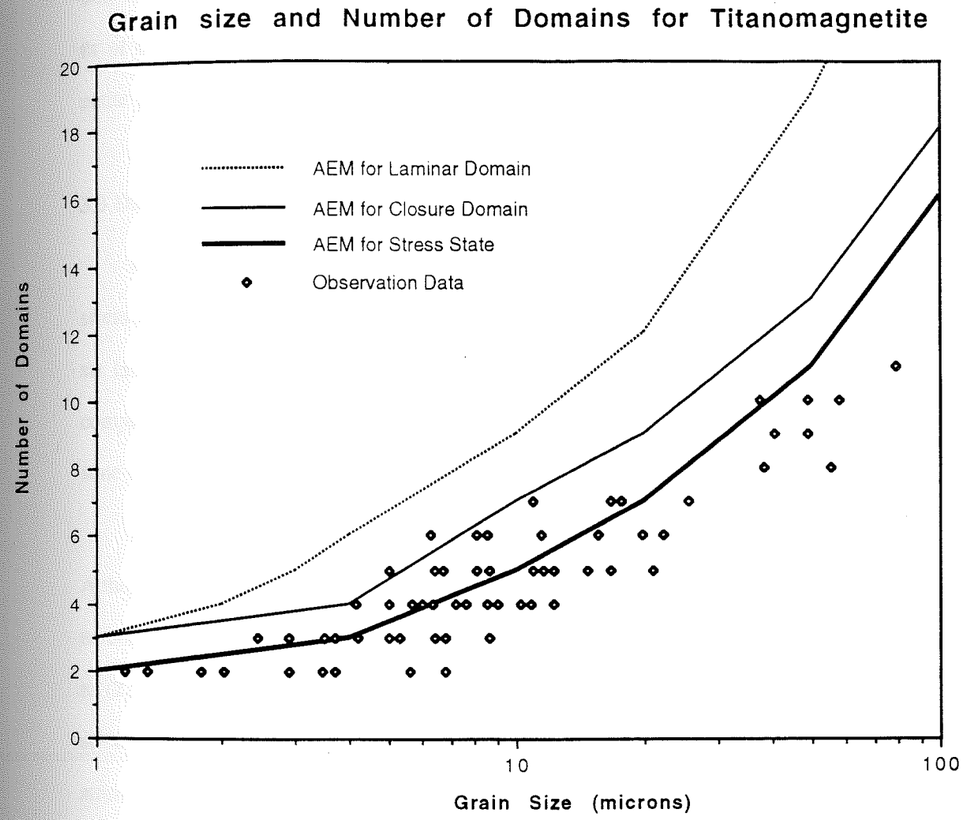

Figure 3.4 The numbers of domains varies with grain sizes for Ti-rich titanomagnetite (TM55). Observation data are from Soffel (1971).

8/14/5

Since the domain state shown in figure 4.12 is a stable state at room temperature, the total magnetic energy of the state should be minimum and any change in the domain state would result in higher energy. This means one should expect $\frac{\partial E_t}{\partial x} = 0$ for A, B, and C residual domains. But we get $\frac{\partial E_t}{\partial x}$ being larger than zero for all three residual domains when we use (4.30) for the gradient of total energy (table 4.1). The non-zero values in table 4.1 are not caused by errors in the calculations because: (1) all the values in table 4.1 are larger than zero (while for calculation errors, both negative and positive values expected) and (2) $\frac{\partial E_t}{\partial x}$ values have the same order of magnitude as $\frac{\partial E_w}{\partial x}$ and $\frac{\partial E_m}{\partial x}$ (not shown) (note for calculation errors, at least one order of magnitude smaller $\frac{\partial E_t}{\partial x}$ than $\frac{\partial E_w}{\partial x}$ and $\frac{\partial E_m}{\partial x}$ is expected since its true value should be zero).

The positive values of $\frac{\partial E_t}{\partial x}$ in table 4.1 indicate that domain A, B, and C should continue to denucleate since the total energy decreases with x decreasing. This apparent contradiction can be explained if defects stop the denucleation process by pinning walls. This implies that the wall energies for domains A, B and C are different from the usual wall energies. Let e'_w denote the wall energy (per unit area) of residual domain walls, and L_{rw} denote the wall length for a residual domain wall. Then, the wall energy is:

$$E_w = E_{w0} + E_{rw} = E_{w0} + D_z \int_{L_{rw}} e'_w dl = E_{w0} + \overline{e'_w} L_{rw} D_z \tag{4.32}$$

Where E_{rw} is the energy of the residual domain wall being considered, and E_{w0} is the energy of the other walls, which does not vary with x. The integral in (4.32) is over the residual domain wall and $\overline{e'_w}$ is the average value of e'_w for the whole wall. The gradient of total energy with respect to x therefore is:

$$\frac{\partial E_t}{\partial x} = \overline{e^{\leftarrow}_w} D_z \frac{\partial L_{rw}}{\partial x} + D_z L_{rw} \frac{\partial \overline{e^{\leftarrow}_w}}{\partial x} + \frac{\partial E_m}{\partial x} \tag{4.33}$$

We define $\overline{\Delta e_w} \equiv \overline{e^{\leftarrow}_w} - e_w$ as the difference between the average wall energy (per unit area) of a residual domain wall and the regular wall energy. By requiring (4.33) to be zero at the reference (observed) state and comparing (4.33) to (4.30) (also notice that $\frac{\partial L_w}{\partial x} = \frac{\partial L_{rw}}{\partial x}$ and $\frac{\partial \overline{e^{\leftarrow}_w}}{\partial x} = \frac{\partial \overline{\Delta e_w}}{\partial x}$), we have

$$\frac{\partial E_d}{\partial x} = D_z L_{rw} \frac{\partial \overline{\Delta e_w}}{\partial x} + D_z \overline{\Delta e_w} \frac{\partial L_{rw}}{\partial x} \tag{4.34}$$

is equal to the negative of the values in table 4.1 for residual domain A, B, and C. E_d is the magnetic energy associated with the defects. The gradient of E_d therefore can be considered as the wall pinning force associated with the defects. In general, the sources of E_d will vary depending on the type of the defects. For example, E_d will be associated with magnetoelastic energy if the defects are dislocations, since dislocations generate a stress field within the grain. In contrast, E_d will be a combination of magnetostatic energy, exchange energy and anisotropy energy if the defects are volume defects (e.g. a cavity).

Contributions to the domain wall pinning force ($\frac{\partial E_d}{\partial x}$) come from two parts. The first part comes from the spatial variation of the average wall energy density (wall energy per unit area) and is given by the first term of (4.34), while the second part comes from the variation of the wall area and is given by the second term of (4.34).

In the following, we assume the pinning forces originate from dislocations and we use the values of $\frac{\partial E_d}{\partial x}$ for residual domain A, B and C to estimate the magnitude of the defects.

First we review some theoretical calculations for the magnetic energy associated with dislocations. The details of the derivation of most of the equations given below can be found in Xu and Merrill (1989) and Xu (1989).

Suppose an edge dislocation (with $\vec{b}$ as its Burgers vector and l as its length) exists in an infinitely large grain, under the rigid wall assumption (meaning that domain wall structure is not affected by the dislocation), the extra wall energy (for a 180° Bloch wall) associated with the dislocation is:

$$\Delta E_w = -\frac{2}{3}\mu blw\,(\lambda_{111}+0.5\lambda_{100})(tanh\frac{x}{w}+2\sqrt{2}sech\frac{x}{w}) \tag{4.35}$$

Where μ is the shear modulus, w is the wall thickness, λ_{111} and λ_{100} are the magnetostriction constants in [111] and [100] directions respectively, and x is the distance from the wall center to the dislocation. The gradient of the energy with respect to x therefore is (assuming that the wall area does not change):

$$\frac{\partial \Delta E_w}{\partial x} = \frac{2}{3}\mu bl\,(\lambda_{111}+0.5\lambda_{100})sech\frac{x}{w}(-sech\frac{x}{w}+2\sqrt{2}\tanh\frac{x}{w}) \tag{4.36}$$

For a screw dislocation, (4.35) becomes

$$\Delta E_w = \mu blw\,\lambda_{111}(sech\frac{x}{w}-2\sqrt{2}\tanh\frac{x}{w}) \tag{4.37}$$

and (4.36) becomes

$$\frac{\partial \Delta E_w}{\partial x} = -\mu bl\,\lambda_{111}sech\frac{x}{w}(tanh\frac{x}{w}+2\sqrt{2}sech\frac{x}{w}) \tag{4.38}$$

Notice that (4.35) and (4.37) are the magnetic energy of the entire wall associated with the dislocation. So in the case we are considering, $D_z L_{rw}\overline{\Delta e_w} = \Delta E_w$. Also notice that (4.36) and (4.38) were derived assuming that the wall area does not change. Therefore we have $D_z L_{rw}\frac{\partial \overline{\Delta e_w}}{\partial x}$ equal to $\frac{\partial \Delta E_w}{\partial x}$ in (4.36) and (4.38). Then for an edge dislocation, we can rewrite (4.34) as

$$\frac{\partial E_d}{\partial x} = \frac{2}{3}\mu bl(\lambda_{111}+0.5\lambda_{100})\left[sech\frac{x}{w}(-sech\frac{x}{w}+2\sqrt{2}\tanh\frac{x}{w})-(tanh\frac{x}{w}+2\sqrt{2}sech\frac{x}{w})\frac{w}{L_{rw}}\frac{\partial L_{rw}}{\partial x}\right] \quad (4.39)$$

For a screw dislocation, (4.34) becomes

$$\frac{\partial E_d}{\partial x} = \mu bl\lambda_{111}\left[-sech\frac{x}{w}(tanh\frac{x}{w}+2\sqrt{2}sech\frac{x}{w})+(sech\frac{x}{w}-2\sqrt{2}\tanh\frac{x}{w})\frac{w}{L_{rw}}\frac{\partial L_{rw}}{\partial x}\right] \quad (4.40)$$

(4.39) and (4.40) explicitly show that the spatial gradient of the energy associated with the dislocation is related to the magnitude of the dislocation (characterized by bl) and the distance between the all center and the dislocation x. Since we only have the value of λ_s for AMTM60 (see, table 3.2), we will use $\lambda_{111} = \lambda_{100} = \lambda_s$ as an approximation in subsequent calculations. The wall width of the sample is about $0.17\mu m$ in stripe domain structures (Moskowitz etc., 1988). By using (4.39) and (4.40), we can get trade off curves for the magnitude of the dislocation (bl) versus the distance the dislocation is from the wall center. Figure 4.13 shows such trade off curves for an edge dislocation and a screw dislocation for residual domain A.

From figure 4.13, one can clearly see that a dislocation with magnitude of bl larger than a minimum value will pin the domain wall at certain point x. Therefore the calculation above gives the minimum value of bl for a dislocation that could pin the wall. For a single edge or a screw dislocation, the magnitude of the Burgers vector is $\frac{\sqrt{2}}{2}a$ with a being the lattice constant of the crystal (see, e.g. Xu, 1989). Since there is no data of a for AMTM60 sample, the value for TM60, which is a=8.485Å, is used(O'Reilly, 1984). This gives b=6.0Å. Then from the minimum values of bl for residual domains A, B, and C, we get the minimum possible values of dislocation lengths (l) for edge and screw dislocations, and these are given in table 4.2. From table 4.2, one can see that the minimum length of the dislocation is about the same in magnitude as the grain size (about $40\mu m$) for an edge dislocation and roughly half of the grain size for a screw dislocation. This indicates that a single

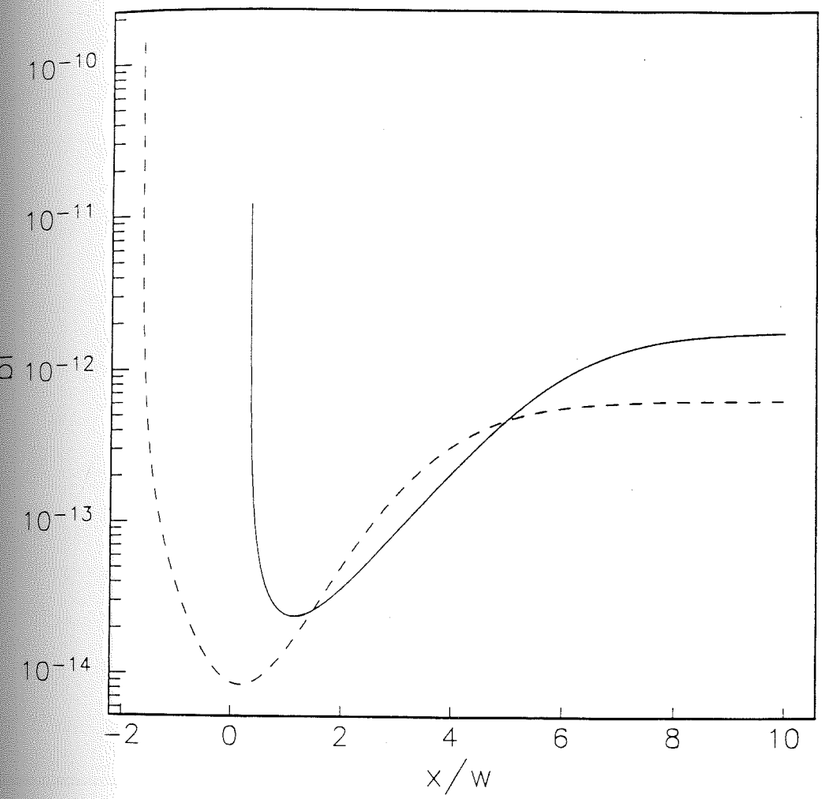

Figure 4.13 x/w and bl (in units of m^2) trade-off curve for domain A. The solid line is for an edge dislocation and the dashed line is for a screw dislocation.

Table 4.2 The minimum lengths of dislocations, l (in μm), for residual domains A, B, and C.

	A	B	C
edge dislocation	39.	58.	51.
screw dislocation	14.	21.	18.

dislocation could be responsible for pinning the domain wall and that a dislocation (especially an edge dislocation) with a small length relative to the grain size, it could not effectively pin the domain wall.

4.7.3 The General Domain Wall Pinning Force from Defects

In general, domain wall pinning force from defects originates from two effects. The first is the spatial gradient of the extra wall energy (per unit wall area), i.e. $\frac{\partial \overline{\Delta e_w}}{\partial x}$, and the second is the spatial gradient of the area of th pinning wall (noted as S_w), i.e. $\frac{\partial S_w}{\partial x}$. Thus the spatial gradient of the extra energy associated with defects (domain wall pinning force) is

$$\frac{\partial E_d}{\partial x} = S_w \frac{\partial \overline{\Delta e_w}}{\partial x} + \overline{\Delta e_w} \frac{\partial S_w}{\partial x} \tag{4.41}$$

In special cases, the wall area, S_w, does not vary spatially and therefore the second term in (4.41) vanishes. However, in general one has to consider the contribution of the second term. In particular, the area of the wall surrounding a domain will change when nucleation or denucleation occurs. Therefore the second term in (4.41) is required here. Obviously, the relative magnitudes of the two term in (4.41) depend on the type of the defects and the geometry of the wall, and it is not the goal of this thesis to delineate all special cases. In the later part of this section, we will show the effect the $\frac{\partial S_w}{\partial x}$ term has in the examples of the residual domains A, B, and C.

From (4.34), the area of the pinning wall is $S_w = D_z L_{rw}$ and $\frac{\partial S_w}{\partial x} = D_z \frac{\partial L_{rw}}{\partial x}$, for constant D_z. The first term in (4.39) comes from the contribution of the gradient of $\overline{\Delta e_w}$ and the second term comes from the contribution of the variation in wall area. Figure 4.14 compares the effects of the two terms on the trade-off between bl and x/w for the domain A

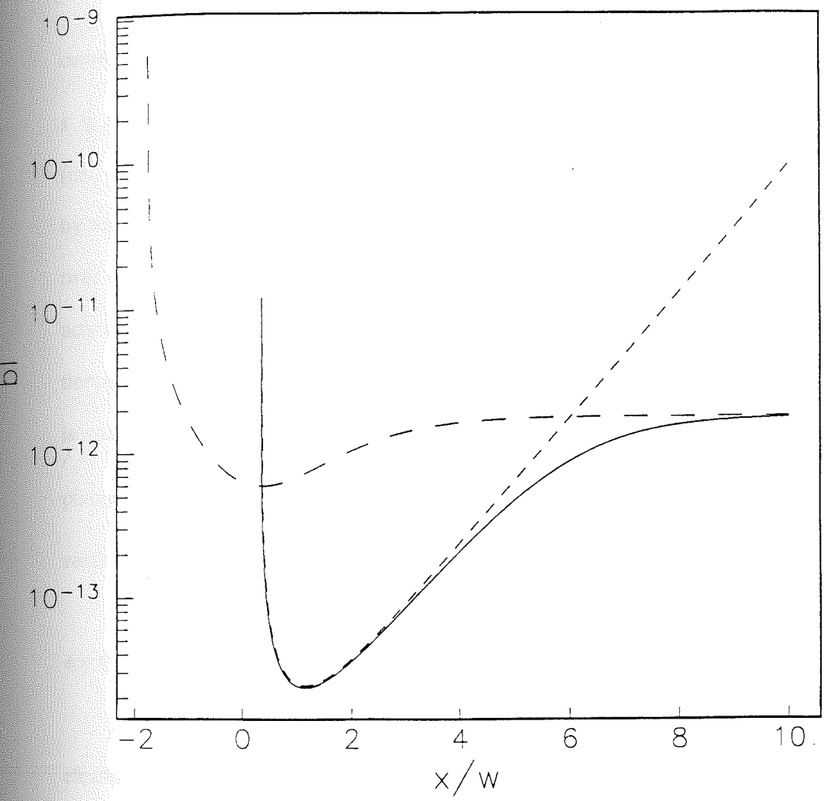

Figure 4.14 x/w and bl (in units of m^2) trade-off curve for domain A with an edge dislocation. The solid line comes from figure 4.14. The short dashed line was calculated using only the $\frac{\partial \overline{\Delta e_w}}{\partial x}$ term in (4.39). The long dashed line was calculated using only the $\frac{\partial L_{rw}}{\partial x}$ term.

case with an edge dislocation. Figure 4.14 shows that when the distance between the dislocation and the wall is small ($x<5w$), the $\frac{\partial \overline{\Delta e_w}}{\partial x}$ term dominates the shape of the trade-off curve, while when the distance is large, the $\frac{\partial S_w}{\partial x}$ term dominates. This illustrates that when x is small, most of the domain pinning force is from the variation in wall energy density (i.e., wall energy per unit area); in contrast, when x is large the pinning force is dominated by the variation in wall area. Therefore there are two kinds of wall pinning forces: one acts over short distances and originates from the variation in wall energy density and the other acts over long distances and is caused by the variation in wall area. It is also worth mentioning that the short range pinning force is more effective than the long range one when x is small ($x<6w$). This becomes clear when one notices that to generate the same value of pinning force ($\frac{\partial E_d}{\partial x}$ in (4.39)), the length of dislocation (l) required is much lower if x is small than that if x is large.

4.8 Conclusions

A one dimensional model has been used in investigating exterior and interior denucleation processes. For large grains ($D>1\mu m$), if there is no external field, the exterior denucleation process has a lower energy barrier than that for interior denucleation. Transdomain processes are improbable for a defect free grain at a constant temperature in a zero external field.

External field, temperature, macrostresses, defects, and grain shape are important factors for transdomain processes. Whether interior or exterior denucleation occurs depends on the grain shape and variations in the external magnetic field. For Ti-rich titanomagnetite, larger macrostress stabilized the distribution in the number of domains with varying temperature. For samples with low macrostress, transdomain processes are more likely during

changes in temperature because domain wall energy changes much faster with temperature than does magnetostatic energy. For Ti-poor titanomagnetite, transdomain processes are more likely to occur relative to Ti-rich titanomagnetite with varying temperature (even with large macrostresses). Defects affect transdomain processes in two different ways. First, defects can pin domain walls (as recognized before). This effect is a short range effect. Second, defects (e.g. dislocations) alter the domain wall energy density and therefore they affect transdomain processes (note that transdomain processes must be accompanied by a change in domain wall area). This effect is a long range effect.

Through numerically simulating three observed domain denucleation processes, the lengths of dislocations were estimated. The results indicate that for Ti-rich titanomagnetite (e.g. AMTM60), it is possible that a single dislocation pins a domain wall. For Ti-poor titanomagnetite, because magnetocrystalline anisotropy plays a more important role in domain structure, a much longer dislocation line seems required to pin a domain wall. The length is so long that in this case a single dislocation may not be the source of domain wall pinning.

CHAPTER 5

APPLICATION OF RENORMALIZATION METHODS TO PREDICT DOMAIN STRUCTURES

In this chapter, we will first discuss some recent results from domain pattern observation and show that the results cannot be explained by current domain theory. Renormalization group theory will be introduced to explain the results. In the later part of this chapter, some applications of the theory will be discussed.

5.1 Observation Results

Halgedahl (1991) observed the number of domains at room temperature for TRM in three AMTM60 grain samples (after cooling the samples from Curie temperature in a weak external field of $0.42Oe$) and after AF demagnetization. By repeating the same procedure several times, a range in the number of domains for each sample was obtained. As shown in figure 5.1, 5.2, 5.3, for three AMTM60 grains with different grain sizes, the ranges of observed number of domains for TRM (with H_{ex}=$0.42Oe$) are much wider than that after AF demagnetization. Since in the process of AF demagnetization, the magnitude of external acting field is gradually reduced, it is reasonable to believe that the distribution of domains after AF demagnetization is centered on the AEM state of the crystal. For the three samples, the AEM states are all about five domains. The number of domains for TRM is in a broader range (relative to the AF case) centered about the AEM state.

5.2 The Failure to Explain the Results by Applying Current Domain Theory

In this section, we investigate the observational results of Halgedahl using current domain theory. We show that the distributions in the number of domains observed at room temperature for TRM are actually determined at temperatures near the Curie temperature at

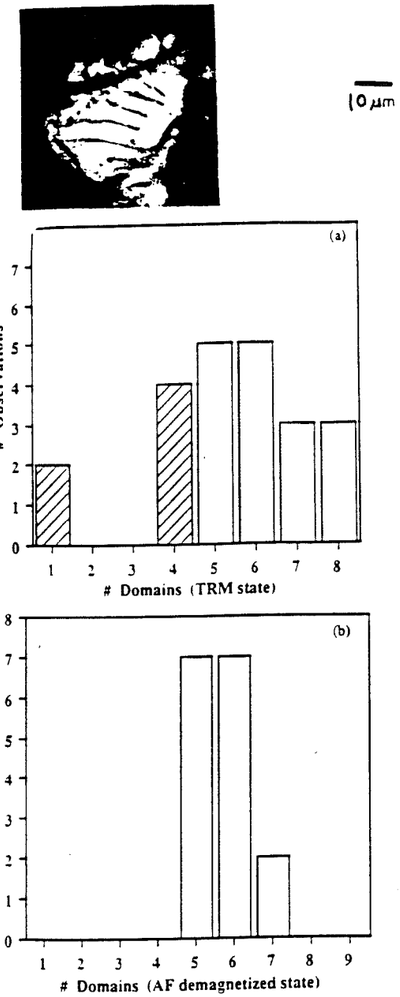

Figure 5.1 The observed number of domains given by Halgedahl (1991) for a AMTM60 grain. (a): the numbers of domains observed for TRM; (b): the numbers of domains observed after AF demagnetization.

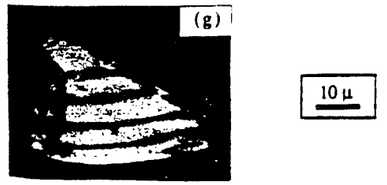

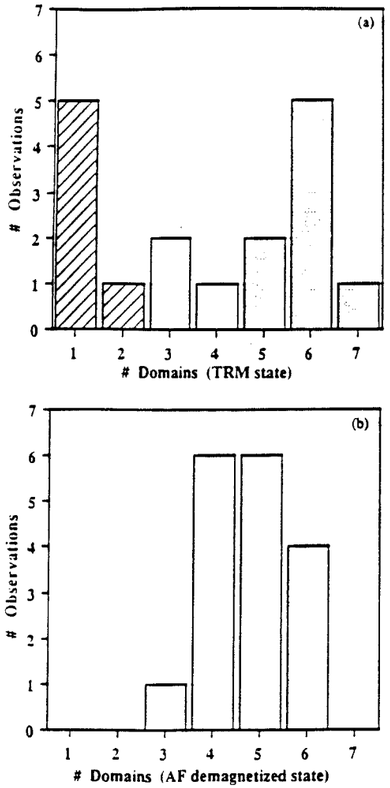

Figure 5.2 The observed number of domains given by Halgedahl (1991) for a AMTM60 grain. (a): the numbers of domains observed for TRM; (b): the numbers of domains observed after AF demagnetization.

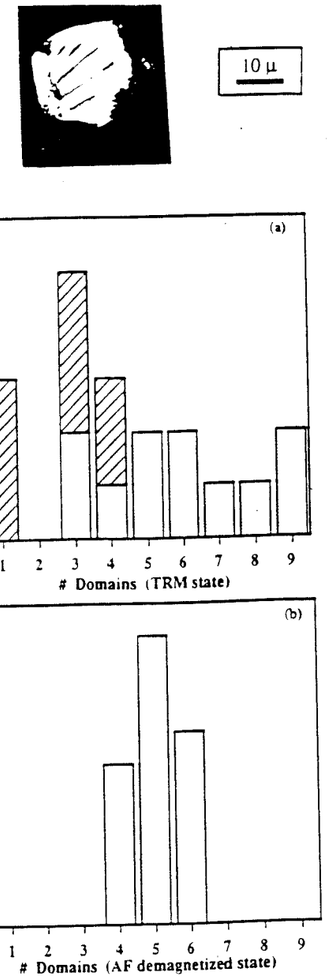

Figure 5.3 The observed number of domains given by Halgedahl (1991) for a AMTM60 grain. (a): the numbers of domains observed for TRM; (b): the numbers of domains observed after AF demagnetization.

which classical domains are not yet formed.

5.2.1 The Possibility of Trans-Domain Processes

First we will show that the observed distributions of number of domains for TRM are not the equilibrium distribution of the samples. For the sample shown in figure 5.3, we can estimate the energy of each state with number of domains being 1,2,...,9. We have chosen the grain shown in figure 5.3 as an example of energy estimation because the grain has roughly equal dimensions and some of the equations in chapter 4 can be used. As an approximation, we consider a grain with cubic shape and laminar domain structure. The total magnetic energy of a state with N domains is: (see, 4.23)

$$E_t = (N-1)e_w D^2 + f_m(N) M_s^{\,2} D^3 \tag{5.1}$$

The first term is the magnetostatic energy and the second term is the domain wall energy. $f_m(N)$ is given in figure 4.9. With $e_w = 1.1\times10^{-3} J/m^2$ (table 3.4) and $D=20\mu m$ (the average value of the grain's length and width), the total magnetic energy of each domain state is shown in figure 5.4. Note that the energy differences between the states is about $10^{-13}J$ to $10^{-12}J$. Note that the external field energy is not included in (5.1), because of its relatively small value (the maximum value of external field energy is $H_{ex}M_sD^3$ which is about $2\times10^{-14}J$ for $H_{ex}=0.42Oe$). For comparison, the thermal fluctuation energy (kT) at room temperature is about $4.\times10^{-21}J$. Since the energies in LEM states are very high with respect to the AEM state, the grain has a small chance to be in any LEM state if the equilibrium state is reached. Therefore the observed wide range in number of domains indicates the grain is not in equilibrium at room temperature. In fact, it was reported that the number of domains observed in each cooling process only rarely changed during cooling the samples from the Curie temperature to room temperature (Halgedahl, 1991).

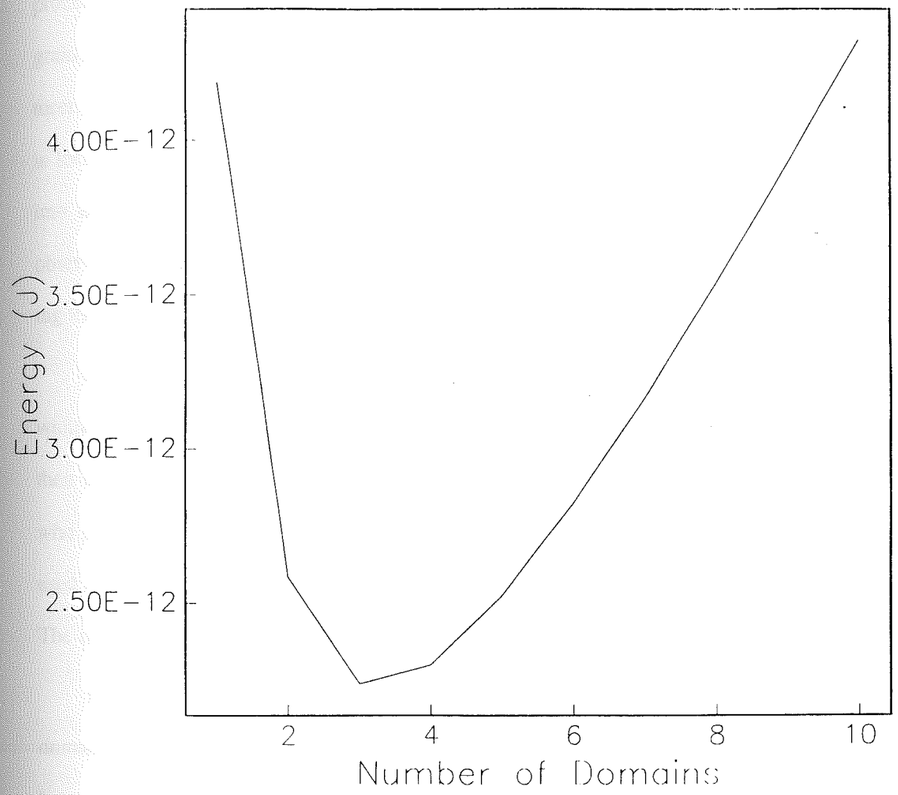

Figure 5.4 The total magnetic energies versus the number of domains for a 20μm cubic AMTM60 grain at room temperature.

5.2.2 Corkscrew Domain Structure

Since the observed distributions of number of domains is not caused by trans-domain processes, logically one would think that there is a relative high temperature at which the grain is in its equilibrium. The possible equilibrium states for a grain varies with temperatures. By gradually cooling, the activation energies between the states increase and the grain is locked into one of these possible states. There is a possibility that a grain can be locked into any of the high temperature LEM states available to the grain. Therefore one might observe a range of domains at room temperature. This possibility will be tested by examining the probabilities associated with occupying different high temperature LEM states.

Xu and Merrill (1990) and Shcherbakov *et al.* (1991) have shown that domain wall widths increases with temperature until adjacent wall "touch." The domain wall structure then becomes continuous throughout the grain. Calculations by Argyle and Dunlop (1984), who used the Amar type wall (laminar domain wall), showed similar results. Moon (1991) used a corkscrew domain structure to describe the magnetic structures at high temperatures. The corkscrew structure model is as follows (for detail, see Moon (1991).

For corkscrew structures, domains and walls are continuous, i.e. there are no classical domains or walls. If the direction of magnetization is within a $y-z$ plane and the angle between the magnetization and z axis is ϕ, the corkscrew structure can be expressed as

$$\phi(x) = s\pi(x/D_x)+\phi_0 \tag{5.2}$$

Where D_x is the grain length in the x direction, s is a parameter which determines how many times the magnetization rotates through π radians within the length of the grain, and ϕ_0 is ϕ at x=0.

Following Moon (1991), the total magnetic energies of a cubic grain (including exchange energy, magnetic anisotropy energy, external field energy and magnetostatic energy) with corkscrew structure is

$$E_t = E_e + E_a + E_h + E_m \tag{5.3}$$

$$= A\pi^2 s^2 D - \frac{1}{2} K cos(2\phi_0) \frac{sin(s\pi)}{s\pi} D^3 - M_s H_{ex} cos(\phi_0) \frac{sin(s\pi/2)}{(s\pi/2)} + 2M_s^2 D^3/s$$

Where A is the exchange constant, M_s is the saturation magnetization, H_{ex} is the external field and K is the uniaxial anisotropy constant, given by

$$K = |K_1'| + \frac{3}{2}\sigma\lambda_{111} \tag{5.4}$$

with σ being the uniaxial stress along the [111] direction (z axis).

By using the constants given in table 3.2 and the stress value in table 3.4 (the average stress value $170MPa$ was used), we can calculate the magnetic energy for the grain at high temperature. Since we are considering the temperature at which the grain reaches its thermal equilibrium state, we calculate the energy at $74.5°C$, a half of degree below the observed Curie temperature of $75°C$. The total magnetic energy for a $20\mu m$ cubic grain at $74.5°C$ is shown in figure 5.5. According to Moon (1991), parameter s is related to the number of domains (N) at room temperature and is given by $N=s+0.5$, providing transdomain processes are ignorable. From figure 5.5, it is clear that the energy differences between the states with different number of domains are about $10^{-17}J$ in magnitude. If we assume the grain is in its equilibrium state, then we can calculate the probability of the grain having N domains, which is

$$P_N = \frac{1}{\Omega} exp(-E_N/kT) \tag{5.5}$$

Where

$$\Omega = \sum_{i=1}^{i=N_{max}} exp(-E_i/kT) \tag{5.6}$$

Where N_{max} is the possible maximum number of domains. Suppose the AEM state of the grain has N_0 domains. We then have

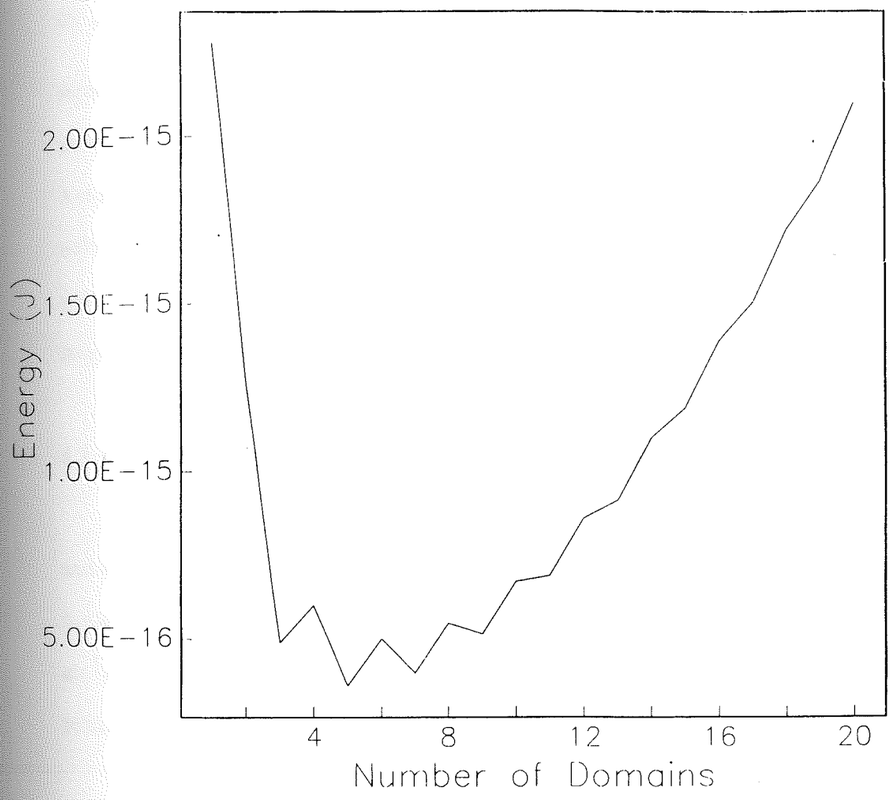

Figure 5.5 The total magnetic energies versus the number of domains for a 20μm cubic AMTM60 grain obtained by using a corkscrew model at 74.5°C.

$$\frac{P_N}{P_{N_0}} = exp\,[-(E_N - E_{N_0})/kT] \tag{5.7}$$

By using $E_N - E_{N_0} \approx 10^{-17} J \approx 2000kT$ at $T=75°C$, for we get $\frac{P_N}{P_{N_0}} \approx exp\,(-2000)$ for $T=75°C$. This means that only N_0 domains should be observed at equilibrium. Therefore the number of domains observed at room temperature is actually determined at even higher temperatures! Yet there is no doubt that classical domain theory is not applicable at these high temperatures since anisotropy energies are negligible at temperatures close to the Curie temperatures. Therefore a new theory must be developed to explain the broad distribution of LEM states observed at room temperature for TRM. temperature.

5.3 The Model of Applying Renormalization Group Theory

The Curie temperature, T_c, is a second order phase transition point for ferromagnetic and ferrimagnetic materials. Such materials exhibit spontaneous magnetization below T_c in the absence of an external magnetic field because of the exchange interaction. These materials do not have any spontaneous magnetization above T_c where they exhibit paramagnetic behavior.

The phase transition between the ferromagnetic (or ferrimagnetic) state and the non-magnetic state is known as a "continuous", or a second order, phase transition because the magnetization goes continuously and smoothly to zero and there is no latent heat which has to be supplied. The two phases never coexist at the same temperature.

From the discussion in the last section, the distribution of the number of domains for TRM appears to be determined primarily at high temperature, i.e., a fraction of a degree below T_c. To test this idea we use techniques similar to those used in renormalization group theory. The advantage of using such techniques is that we do not need to know the detailed nature of the magnetic structure in the temperature range where the temperatures are too

high for classical domain structures to exist. Readers not familiar with this theory are referred to the readable account by Bruce and Wallace (1989). The material presented there is hereafter assumed to be background material for this thesis.

To apply the theory, we divide a grain ($D_x \times D_y \times D_z$) into $N \times M \times L$ cubic clusters in three dimensions with the grid size $d=D_x/N=D_y/M=D_z/L$ (figure 5.6). For simplicity, each small cubic block is assumed to have an uniform magnetization along either $+\vec{Z}$ or $-\vec{Z}$ directions. This model can be called a renormalized Ising model. At a temperature close to the Curie temperature, it is reasonable to assume that the clusters with magnetization along $+\vec{Z}$ and $-\vec{Z}$ are randomly distributed in the grain since the thermal fluctuation energy dominates all the other magnetic energies (i.e., exchange energy, magnetostatic energy, external field energy and magnetic anisotropy energy). As the temperature decreases, the magnetic moments of the clusters will reorganize approaching states commonly observed to have classical domains and walls. In the next section, we will use a method similar to the renormalization group theory to investigate how the state with randomly distributed clusters would transfer to states with 'domain-like' structures.

5.4 The Evolution of Cluster Structures

As well as using renormalization group method, our discussion about the evolution of cluster structures is based on related magnetic energies since at any temperature a system prefers to be in lower energy states.

5.4.1 The magnetic energies

As discussed in chapter 2, the total magnetic energy includes exchange energy, magnetic anisotropy energy (i.e., magnetocrystalline energy and magnetoelastic energy), magnetostatic energy and external field energy. For AMTM60, the exchange energy is

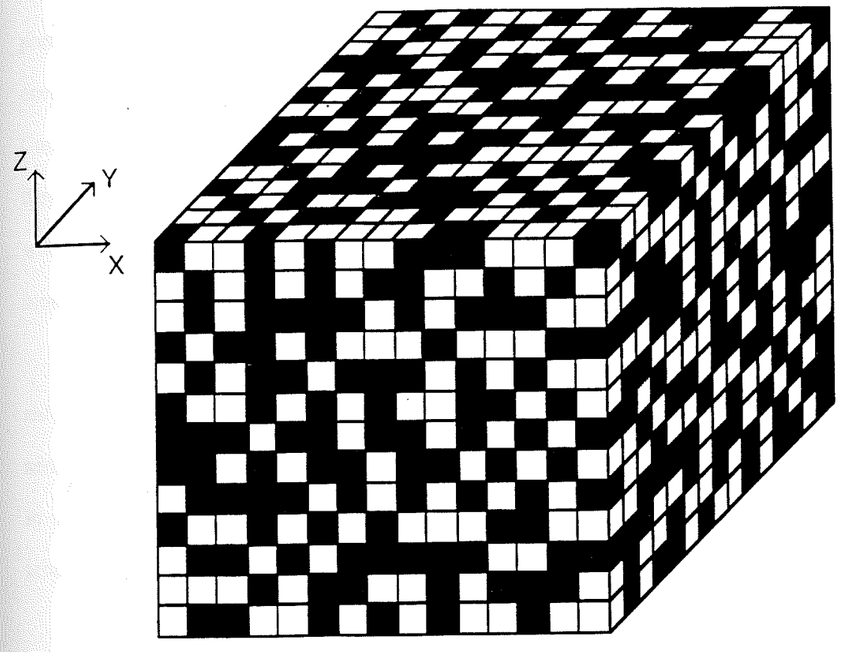

Figure 5.6 Three dimensional renormalized Ising model. The grain is separated to $N \times M \times L$ grids. Black grids have magnetization along $+\vec{Z}$. White grids have magnetization along $-\vec{Z}$.

proportional to the exchange constant A which has a temperature dependence that goes as $M_s^{1.9}$; magnetocrystalline energy is proportional to $K_1' \propto M_s^{10}$; magnetoelastic energy is proportional to $\lambda_s \propto M_s^{2.6}$; magnetostatic energy is proportional to M_s^2; while external field energy is proportional to M_s (table 3.2). For simplicity, at high temperature close to the Curie point, we ignore the magnetocrystalline energy and magnetoelastic energy because they decrease quickly with temperature relative to the other three energies. Although we will not deal with magnetic anisotropy energy hereafter, we still assume that the magnetic moment in each cluster is either along $+\vec{Z}$ or $-\vec{Z}$.

Now let us discuss some features of exchange energy, magnetostatic energy and external field energy. Exchange energy originates from the exchange coupling of adjacent spins and is related to spatial gradients of the magnetization (2.2). Therefore if the magnetization in one cluster is along $+\vec{Z}$ (or $-\vec{Z}$), the magnetic moments in the adjacent clusters have a tendency to be along $+\vec{Z}$ (or $-\vec{Z}$).

Magnetostatic energy originates from the magnetic interactions between the magnetic moments. As shown in figure 5.7, if a cluster has a magnetic moment along $+\vec{Z}$, the magnetic moments of clusters which locate along Z axis have a tendency to align along $+\vec{Z}$ axis while the magnetic moments of clusters which locate on $X-Y$ plane have a tendency to align $-\vec{Z}$.

If an external magnetic field, along $+\vec{Z}$ for instance, acts on a grain, the magnetic moments of all clusters have a tendency to align parallel to the field since this gives rise to the lowest energy state.

5.4.2 The Initial State of The Cluster Structure

We will consider two cases for a system (a grain): one with an external field and the other without an external field.

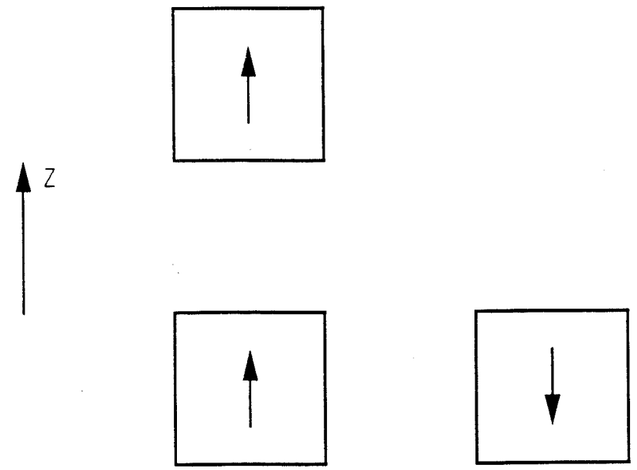

Figure 5.7 The figure illustrates that for lower magnetostatic energy, (two) grids along the Z axis have a tendency to have same polarity, in contract, (two) grids in the $X-Y$ plane have a tendency to have the opposite polarities.

For the case without the external field, a cluster has an equal probability to have its magnetization along $+\vec{Z}$ or $-\vec{Z}$. If we denote the probabilities to have the magnetization along $+\vec{Z}$ and $-\vec{Z}$ as p_+ and p_- respectively, we have

$$p_+ = p_- = 0.5 \tag{5.8}$$

For the case with external field H_{ex} along $+\vec{Z}$ (for simplicity, this is the only field direction considered), clusters have more chance to have magnetic moments along $+\vec{Z}$ than along $-\vec{Z}$, i.e., $p_+ > p_-$. We define a bias rate, b, as that part of p_+ which is more than 0.5. That means

$$p_+ = 0.5+b \ , \quad \text{and} \quad p_- = 0.5-b \tag{5.9}$$

The bias rate, b, is caused by H_{ex} and related to other parameters such as the volume of the cluster. More discussion of this will be given later. For the case without an external field, b is zero.

5.4.3 The First Step of Renormalization

In the following, we discuss the evolution of clusters and the formation of 'domain-like' structures. We use ideas similar to those used in the renormalization group method, i.e., the averaging out of fluctuations in steps. During each step fluctuations are averaged over a certain space scale. This continues until the fluctuations on all scales averaged out and a macro-quantity is obtained. We average out the magnetization in all clusters of the grain by three steps. In each step, we average the magnetization of clusters along one dimension.

In the first step, we average the magnetizations of clusters along the Z axis. Either the exchange energy or the magnetostatic energy would prefer that all the clusters have the same direction of magnetization along Z axis.. Therefore it is obvious that the two states for

which all the clusters along the Z axis have the same polarity of magnetization (+1 or −1) are the lowest energy states. Thus, for each column along the Z axis, there is a unique polarity, +1 or −1. To determined whether the magnetization is along $+\vec{Z}$ or $-\vec{Z}$, we use the following rule. If initially there are more clusters with +1 magnetization than that those with −1 in the column, then the polarity of the entire column is set to +1 (and vice versa). This is obviously a reasonable rule since it means that the polarity of the column is determined by the majority. For the case when an external field is present, we have $p_+ > p_-$. Then in general there are more columns with positive polarity than with negative polarity in the total $M \times N$ columns. In order to avoid the case where there are equal numbers of (+) and (–) clusters in one column and then the polarity of the column cannot be determined by the rule, the total number of clusters in each column, L, is required to be an odd number.

The probability of having (+) magnetization in each column is:

$$p'_+ = \sum_{i=0}^{(L-1)/2} C_L^i \, p_-^i \, p_+^{L-i} \tag{5.10}$$

And $p'_- = 1 - p'_+$. After renormalized the magnetization in each column, we get two dimensional $M \times N$ clusters with probabilities of (+) and (–) polarities given above. For the case of no external flied, $p'_+ = p'_- = 0.5$.

5.4.4 The Second Step of Renormalization

In the second step, we renormalize the polarities of the clusters along the Y axis. Although this step of renormalization is artificial, the following discussion gives some physical reasons for it.

It is convenient to use figure 5.8 to explain our concern. Suppose there are two adjacent clusters with the same polarity (+). The exchange interaction acts to align the magnetization of the adjacent cluster to be along (+). The clusters along the line formed by the two

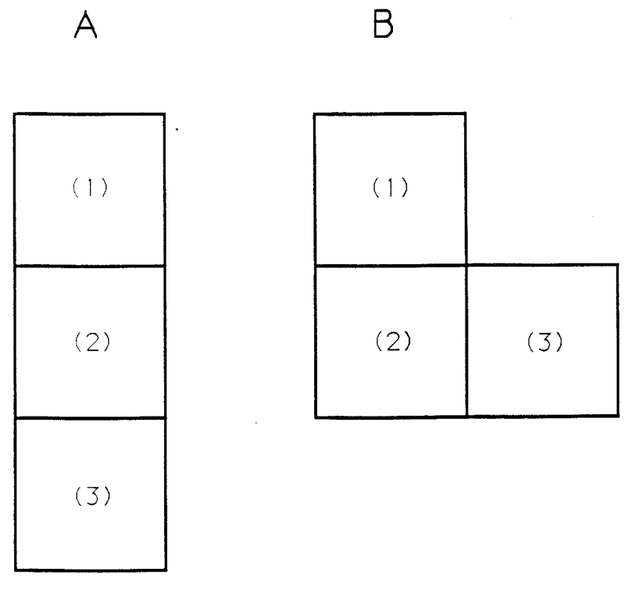

Figure 5.8 The figure illustrates that for the case in which two (or more) grids have formed one line, if exchange energy converts another grid to join this cluster, the grid along the line will change its polarity. Case A has a lower mutual magnetostatic energy between grid (1) and grid (3) than that for case B, because of the larger distance between (1) and (3) (eventhough the other parts of the total energy is the same for two cases).

clusters with (+) polarity have a higher probability to change (or retain) their polarity to (+) because of the magnetostatic energy. This tendency increases when more clusters along one line have same polarity. Therefore there is a tendency for clusters of the same polarity to align along lines. Based on this, and because we compare our results to laminar domain structures, the second step of renormalization will be along the Y axis.

Because the polarity of a column depends on the polarities of the clusters within this column as well as the polarities of the neighbor columns, we will use the following rule to determine the polarity of each column along Y axis. Let denote S as the summation of the magnetic moments along a column. The rule is: if S is larger than or equal to a critical value S_c, then the column has (+) polarity; in contrast, if S is less than or equal to $-S_c$, then the column has (–) polarity; if $-S_c < S < S_c$, then the polarity of the column is considered to be neutral and denoted as (0). The polarity of those (0) columns will be determined in the next step of renormalization. S_c is a adjusting parameter and will be discussed later.

Since there are M clusters in a column along the Y axis, S has $M+1$ possible values. They are $-M$, $-(M-2)$, ..., $M-2$, M. If the summation of magnetic moments in a column is S, there are $(M-S)/2$ clusters with (–) polarity in the column and $(M+S)/2$ cluster with (+) polarity. If we denote the number of (–) clusters in a column as j and $j_c = (M-S_c)/2$ as the number of (–) clusters at $S=S_c$, it is easy to calculate the probabilities for each column being (+), (–) or (0). Theses are:

$$P_+ = \sum_{j=0}^{j_c} C_M^j \, p'^j_- \, p'^{M-j}_+$$

$$P_- = \sum_{j=M-j_c}^{M} C_M^j \, p'^j_- \, p'^{M-j}_+ \qquad (5.11)$$

$$P_0 = \sum_{j=j_c+1}^{M-j_c-1} C_M^j \, p'^{\,j}_{-} \, p'^{\,M-j}_{+}$$

where p'_+ and p'_- are given by (5.10).

For the case of no external filed, since $p'_+ = p'_- = 0.5$, we have

$$P_+ = P_- = \frac{1}{2^M} \sum_{j=0}^{j_c} C_m^j \,, \qquad P_0 = 1-2P_+ \tag{5.12}$$

After this step of renormalization, we obtain a one dimensional cluster structure along the X axis with N clusters. The clusters have (+), (–) and (0) polarities with probabilities given by (5.11) and (5.12).

5.4.5 The Third Step of Renormalization

In this step of renormalization, we convert (0) clusters to (+) and (–) regions. Figure 5.9 shows an example of one dimensional clusters with (+), (–) and (0) polarities. There are three kinds of positions of (0) clusters. They are: (1) (0) clusters are between (+) clusters; (2) (0) clusters are between (–) clusters and (3) (0) clusters is between (+) clusters and (–) clusters. For (1) or (2), we will change the polarity of (0) clusters to (+) or (–) respectively (to lower the exchange energy). For case (3), (0) clusters have an equal probability to be (+) or (–). We arbitrarily choose them to have the same sign of polarity as their left non-(0) neighbor. Based on this rule, we can obtain a grain structure separated into (+) and (–) regions (we will call them "predomains"). For a grain with i+1 predomains, there are i boundaries associated across which the polarity changes. Let us call those boundaries "prewalls" (they are not classical domain walls).

In the following, we will calculate the probability for i prewalls. The number of walls could vary from 0 to N–1. There are N–1 possible positions for those prewalls. They are 1, 2, ..., N–1. Let us consider the case when the grain has i prewalls. There are C_{N-1}^i

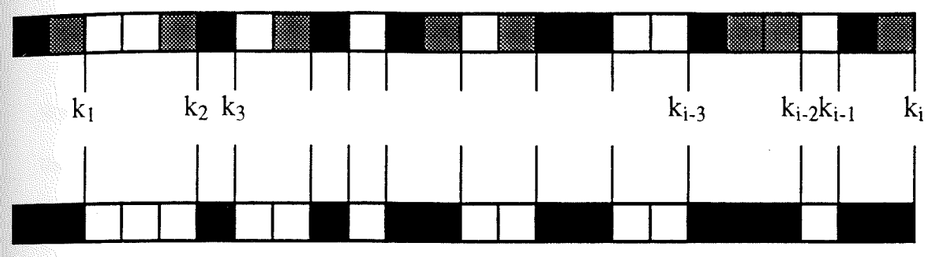

Figure 5.9 This figure illustrates the third step of renormalization: how i predomains forms. The wall positions are at $k_1, k_2, ..., k_{i-1}$. $k_i \equiv N$. Black is (+); white is (−); gray is (0).

ways to put the prewalls in the grain. Suppose the i walls are at k_j, (j=1, ..., i) (figure 5.9). Then the probability there are i prewalls and they are at k_j, (j=1, ..., N–1) is:

$$P_{k_1,\ldots,k_i} = \left[(1-p_-)^{k_1} - P_0^{k_1}\right] P_- (1-P_+)^{k_2-k_1-1} P_+ (1-P_-)^{k_3-k_2-1} \ldots P_{\mp} (1-P_{\pm})^{N-k_i-1} \qquad (5.13)$$

$$+ \left[(1-p_+)^{k_1} - P_0^{k_1}\right] P_+ (1-P_-)^{k_2-k_1-1} P_- (1-P_+)^{k_3-k_2-1} \ldots P_{\pm} (1-P_{\mp})^{N-k_i-1}$$

The two terms in (5.13) is related to the sign of the first predomain (figure 5.9). The first term is the probability the first predomain is (+) and the second term is the probability the first predomain is (–). The first factor in the first term is the probability there are no (–) clusters in the first k_1 clusters and all k_1 clusters are not all (0). The second factor, P_-, arises because the k_1 *th* cluster has to be (–). The third factor reflects there are no (+) between the (k_1+1)*th* cluster and the (k_2-1)*th* cluster, etc. The signs in the last factors of the two terms depend on whether i is an odd or an even number. If i is odd, the lower sign should be used; if i is even, the upper sign should be used.

When there is an external field acting on the grain, $P_+ \neq P_-$ (see 5.11). For even i ($i \geq 2$), (5.13) can be rewritten as

$$P_{k_1,\ldots,k_i} = \left(\frac{P_+}{1-P_+}\right)^{\frac{i}{2}} \left(\frac{P_-}{1-P_-}\right)^{\frac{i}{2}} \left[\left[(1-P_-)^{k_1} - P_0^{k_1}\right] (1-P_+)^m (1-P_-)^{m'} \right. \qquad (5.14)$$

$$\left. + \left[(1-P_+)^{k_1} - P_0^{k_1}\right] (1-P_+)^{m'} (1-P_-)^m \right]$$

with m and m' given by

$$m = \sum_{j=1}^{i/2} (k_{2j} - k_{2j-1}), \quad m' = \sum_{j=1}^{i/2} (k_{2j+1} - k_{2j}) \qquad (5.15)$$

where $k_{i+1} \equiv N$.

For odd i ($i \geq 3$), (5.13) can be written as

$$P_{k_1,\ldots,k_i} = \left(\frac{P_+}{1-P_-}\right)^{(i-1)/2}\left(\frac{P_-}{1-P_+}\right)^{(i+1)/2}\left[(1-P_-)^{k_1}-P_0^{k_1}\right](1-P_+)^m(1-P_-)^{m'} \tag{5.16}$$

$$+\left(\frac{P_+}{1-P_-}\right)^{(i+1)/2}\left(\frac{P_-}{1-P_+}\right)^{(i-1)/2}\left[(1-P_+)^{k_1}-P_0^{k_1}\right](1-P_-)^m(1-P_+)^{m'}$$

with m and m' given by

$$m = \sum_{j=1}^{(i+1)/2}(k_{2j}-k_{2j-1}), \quad m' = \sum_{j=1}^{(i-1)/2}(k_{2j+1}-k_{2j}) \tag{5.17}$$

For both even i and odd i cases, it is easy to prove the relation between m and m' is

$$m + m' = N - k_1 \tag{5.18}$$

According to (5.14) and (5.16), $P_{k_1,\ldots,k_i}$ depends on i, m, k_1 only and does not depend on $k_2, \ldots, k_i$. For i even, the permutation of $k_2, \ldots, k_i$ for constants m and m' given by (5.15) is $C_{m-1}^{i/2-1}\times C_{m'-1}^{i/2-1}$. For i odd, m and m' are given by (5.17) and the permutation of $k_2, \ldots, k_i$ is $C_{m-1}^{(i-1)/2}\times C_{m'-1}^{(i-3)/2}$ (see, Appendix C). For even i, since k_1 can choose any integer from 1 to $N-i$ and the possible values of m are the integers from $i/2$ to $N-k_1-i/2$ (see (5.15) and (5.17), we can obtain the probability of $i+1$ domains as:

$$P_{i+1} = \sum_{k_1=1}^{N-i}\sum_{m=i/2}^{N-k_1-i/2} P_{k_1,\ldots,k_i} \tag{5.19}$$

By using (5.14) and (5.18), we get

$$P_{i+1} = \left(\frac{P_+}{1-P_+}\right)^{\frac{i}{2}}\left(\frac{P_-}{1-P_-}\right)^{\frac{i}{2}}\sum_{k_1=1}^{N-i}\sum_{m=i/2}^{N-k_1-i/2} C_{m-1}^{i/2-1}\; C_{N-k_1-m-1}^{i/2-1}\left[\left[(1-P_-)^{k_1}-P_0^{k_1}\right](1-P_+)^m\right. \tag{5.20}$$

$$\left.(1-P_-)^{N-k_1-m}+\left[(1-P_+)^{k_1}-P_0^{k_1}\right](1-P_+)^{N-k_1-m}\,(1-P_-)^m\right]$$

For odd i, the possible values of m are integers from $(i+1)/2$ to $N-k_1-(i-1)/2$ (see (5.17) and (5.18). The probability to have $i+1$ predomains in the grain is

$$P_{i+1} = \sum_{k_1=1}^{N-i} \sum_{m=(i+1)/2}^{N-k_1-(i-1)/2} P_{k_1, \ldots, k_i} \tag{5.21}$$

By using (5.16) and (5.18), we get

$$P_{i+1} = \sum_{k_1=1}^{N-i} \sum_{m=(i+1)/2}^{N-k_1-(i-1)/2} C_{m-1}^{(i-1)/2} C_{N-k_1-m-1}^{(i-3)/2} \tag{5.22}$$

$$\left\{\left[\frac{P_+}{1-P_-}\right]^{(i-1)/2}\left[\frac{P_-}{1-P_+}\right]^{(i+1)/2}\left[(1-P_-)^{k_1}-P_0^{k_1}\right](1-P_+)^m(1-P_-)^{N-k_1-m}\right.$$

$$\left.+\left[\frac{P_+}{1-P_-}\right]^{(i+1)/2}\left[\frac{P_-}{1-P_+}\right]^{(i-1)/2}\left[(1-P_+)^{k_1}-P_0^{k_1}\right](1-P_-)^m(1-P_+)^{N-k_1-m}\right\}$$

For a single predomain (i.e. i=0), P_1 obviously can be expressed as

$$P_1 = (1-P_+)^N + (1-P_-)^N - P_0^N \tag{5.23}$$

For the two predomain case (i.e. i=1), based on (5.13), we find P_2 is:

$$P_2 = \sum_{k_1=1}^{N-1}\left\{\left[\frac{P_+}{1-P_-}\right]\left[(1-P_+)^{k_1}-P_0^{k_1}\right](1-P_-)^{N-k_1}+\left[\frac{P_-}{1-P_+}\right]\left[(1-P_-)^{k_1}-P_0^{k_1}\right](1-P_+)^{N-k_1}\right\} \tag{5.24}$$

For the case without an external field, $P_+ = P_-$. Therefore (5.13) can be written as

$$P_{k_1, \ldots, k_i} = 2P_+^i(1-P_+)^{N-i}\left[1-\left[\frac{P_0}{1-P_+}\right]^{k_1}\right] \tag{5.25}$$

This means that $P_{k_1, \ldots, k_i}$ is only dependent on i and k_1. Since k_1 is the position of first prewall from the left and there are $i-1$ prewalls on right side of k_1, k_1 has $N-i$ possible values which are 1, 2, ..., $N-i$. For $k_1 = j$ ($1 \le j \le N-i$), there are $N-j-1$ possible prewall positions on the right side of k_1. Therefore the total number of ways to put the other $i-1$ prewalls in the $N-j-1$ possible positions is C_{N-j-1}^{i-1}. The probability of having $i+1$ predomains then is

$$P_{i+1} = 2P_+^i\ (1-P_+)^{N-i}\sum_{j=1}^{N-i} C_{N-j-1}^{i-1}\left[1-\left(\frac{P_0}{1-P_+}\right)^j\right] \tag{5.26}$$

Where P_+ and P_0 are given by (5.12).

In particular, the probability of a single predomain for the case with no external field is (see (5.23):

$$P_1 = 2(1-P_+)^N - P_0^N \tag{5.27}$$

After the third step of renormalization, the grain is separated into $i+1$ ($i=0, ..., N-1$) regions which have uniform magnetization along either $+\vec{Z}$ or $-\vec{Z}$. We call these regions as "predomains". Presumably the magnetic domain structures observed at lower temperatures are developed from these predomains. If transdomain processes are essentially negligible (as observed by Halgedahl (1991), then each "predomain" at high temperature will presumably develop into one classical magnetic domain at low temperature. This means that the number of predomains at high temperatures is identical to the number of classical domains at low temperatures. Therefore (5.20), (5.22), (5.23), (5.24), (5.26) and (5.27) give the probabilities different domain structures will be observed at low temperature for a given size grain.

5.5 Results and Discussion

Based on the formulas developed in last section, the distributions in number of domains depends on the three parameters (i.e., grid size d, bias rate b and a critical value S_c). Further discussion of these parameters is needed.

5.5.1 The Ranges of Parameters

The range of grid size, d, is very wide. The lowest limit of d is certainly the dimension of the unit cell of the mineral. The unit cell dimension is about 8.5Å for TM60 (O'Reilly, 1984) and this is used as an excellent approximation for AMTM60 since *Al* and

Mg are minor constituents. Because the maximum grid size should be significantly less than domain wall width at room temperature, a reasonable upper limit of $0.05\mu m$ is taken.

The bias rate, b, is actually related to gird size, d. If there is no external field, a cluster has equal chance to be (+) or (–). It is the external field that provides the preference for one of the two directions. That is the external field energy is the only energy difference between (+) and (–) clusters. Therefore we can calculate the bias rate for certain value of external field by using Boltzmann statistics. Since we assumed that initially, the system is in thermal equilibrium, we have

$$p_+ = \frac{1}{\Omega}\exp\left[H_{ex}\nu M_s(T)/kT\right], \qquad p_- = \frac{1}{\Omega}\exp\left[-H_{ex}\nu M_s(T)/kT\right] \tag{5.28}$$

Where Ω is the partition function which equals $exp(H_{ex}\nu M_s(T)/kT)+exp(-H_{ex}\nu M_s(T)/kT)$, H_{ex} is the external field and $v = d^3$ is the volume of the clusters. The bias rate, b, therefore equals (see 5.9)

$$b = \frac{\exp\left[2H_{ex}\nu M_s(T)/kT\right]}{1+exp\left[2H_{ex}\nu M_s(T)/kT\right]} - 0.5 \tag{5.29}$$

By using the temperature dependence of M_s shown in table 3.2, b can be calculated for a given field at a given temperature. The variation of b verse d is shown in figure 5.10 for H=0.42Oe (which is the field during the experiments, see section 5.1) and T=74°C. For a given value of d, depending on temperature, b can be chosen as any value from 0 (when $T \rightarrow T_c$) to the value at the line (when T=74°C) in figure 5.10.

The critical value S_c is an artificial parameter which is used to adjust the distribution of number of domains to fit observational data. Therefore the choice of S_c will be considered in a later discussion on the distribution of the number of domains.

5.5.2 The Results for Zero Bias Rate

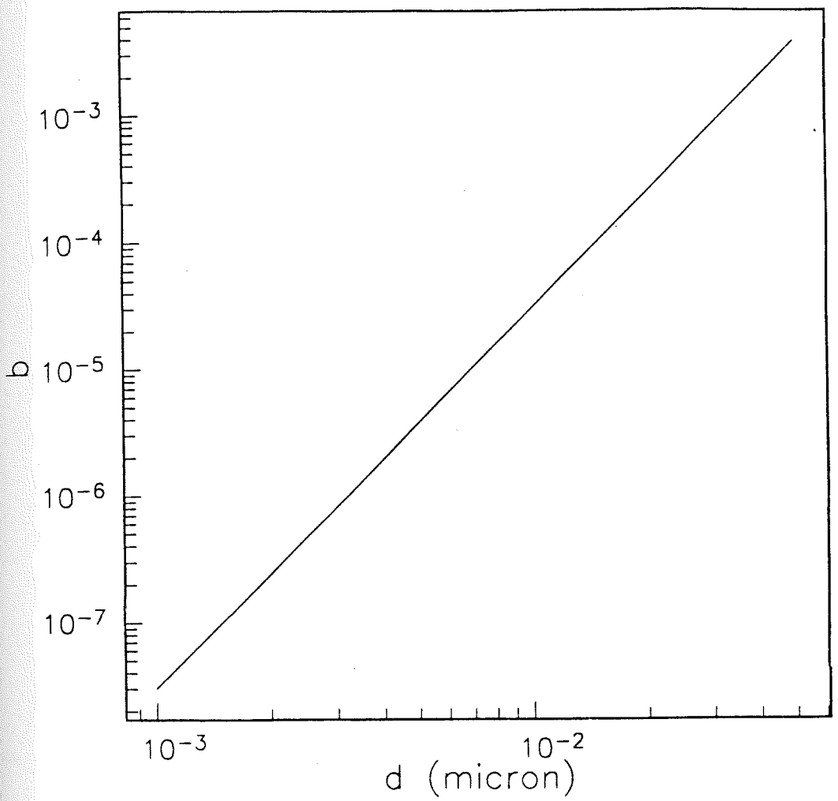

Figure 5.10 The relationship between d and b. The line is for $74°C$. The higher the temperature, the lower the value of b.

Let us first look at the distributions of number of domains for a given size grain at zero bias rate. This is the case for zero external field and the limiting case when $T \to T_c$ (since $M_s \to 0$ when $T \to T_c$).

Consider a grain with size $20\times20\times20\ \mu m^3$, when we choose the grid size corresponding to the minimum limit ($10^{-3}\mu m$), the maximum limit ($5.\times10^{-2}\mu m$) and a medium value (e.g. $2.\times10^{-2}\mu m$), the grain is separated into 20000×20000×20000, 400×400×400 and 1000×1000×1000 grids respectively. For each of these grid sizes, by using (5.26) and (5.27) with an appropriate value of S_c, the number of domains has a similar range to that observed (see figure 5.3, 5.11, 5.12 and 5.13). Figure 5.11, 5.12 and 5.13 also show that once appropriate values of S_c are chosen, the distributions in the number of domains for different gird sizes can be very similar. This similarity indicates that our model is not very sensitive to the grid size. In other words, although we do not have enough information to estimate the grid size precisely, the renormalization group method used can still yield good estimates for distributions of the number of domains.

5.5.3 The Results with a Bias

Since the choice of grid size only slightly affects the distribution in the number of domains, we will discuss the effects of an external field for only one gird size (e.g. $2.\times10^{-2}\mu m$). In order to compare the results with observational data, let us consider the case in which $H = 0.42Oe$ (used in Halgedahl's experiments). Depending on the temperature, the possible range for the bias is from b=0 (at $T \to T_c$) to 2.4×10^{-4} (at T=74°C). By using the same value of S_c used for the zero external field case, the distributions in the number of domains for a $20\times20\times20\ \mu m$ grain are shown in figure 5.14. Figure 5.14 indicates that there are two kinds of effects the external field has on the distribution. These are: (1) external field could shift the range of distribution to a lower number of domains; and (2) external

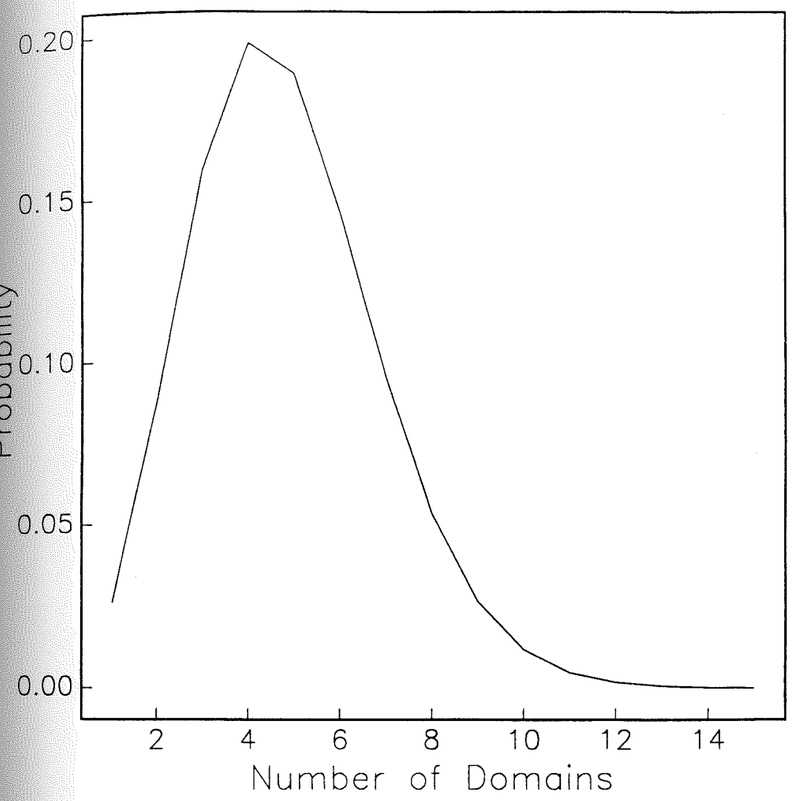

Figure 5.11 The distribution in the number of domains for 20μm grains with grid size 0.05μm and S_c=48. There are 400×400×400 grid cubes in the grains.

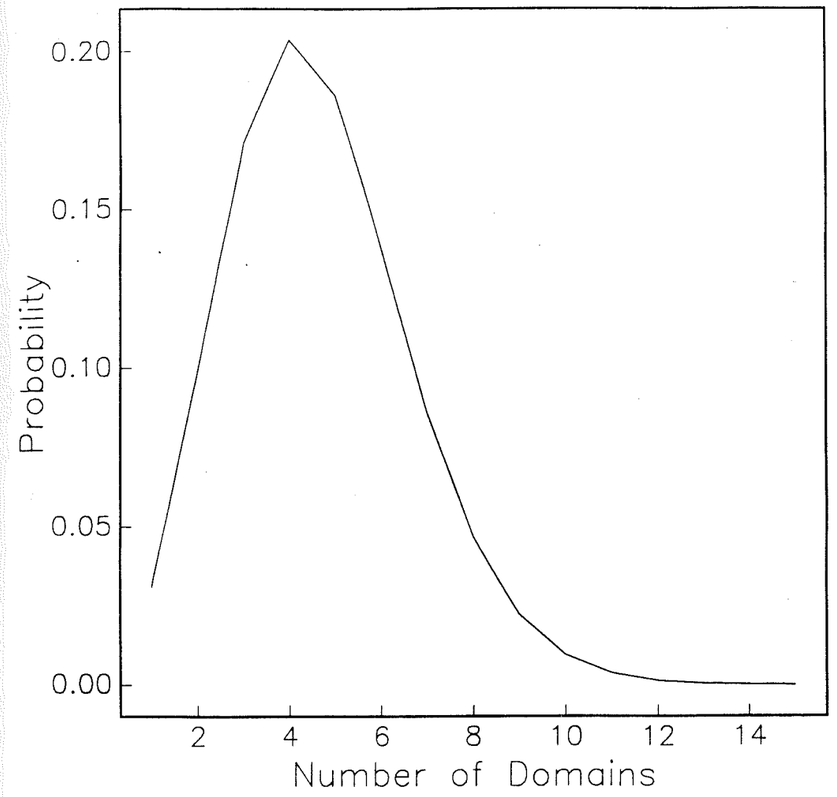

Figure 5.12 The distribution in the number of domains for 20μm grains with grid size 0.02μm and S_c=84. There are 1000×1000×1000 grid cubes in the grains.

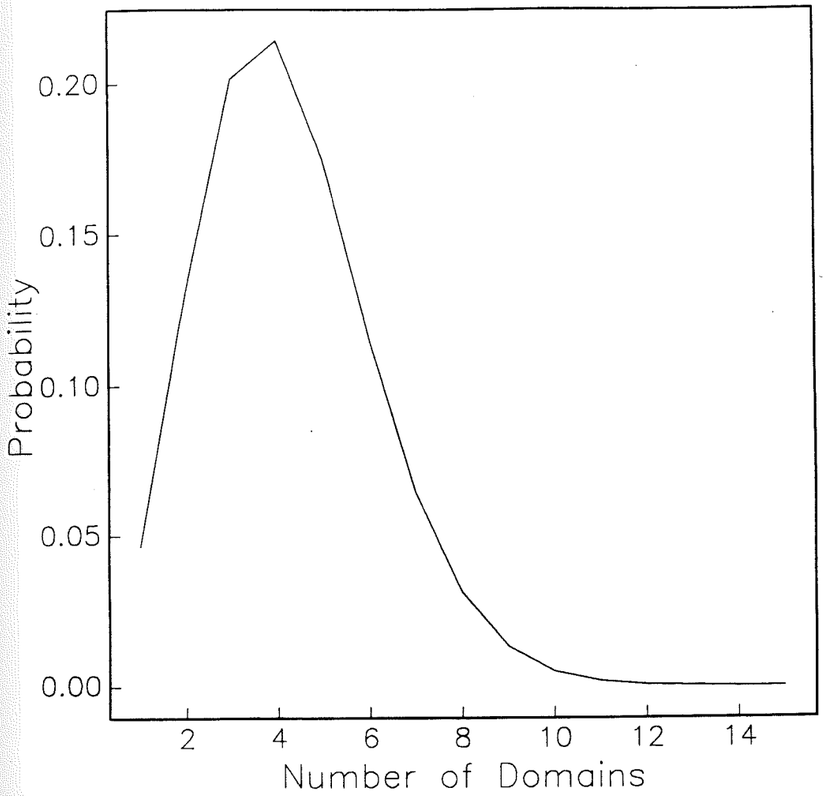

Figure 5.13 The distribution in the number of domains for 20μm grains with grid size $10^{-3}\mu m$=10Å and S_c=500. There are 20000×20000×20000 grid cubes in the grains.

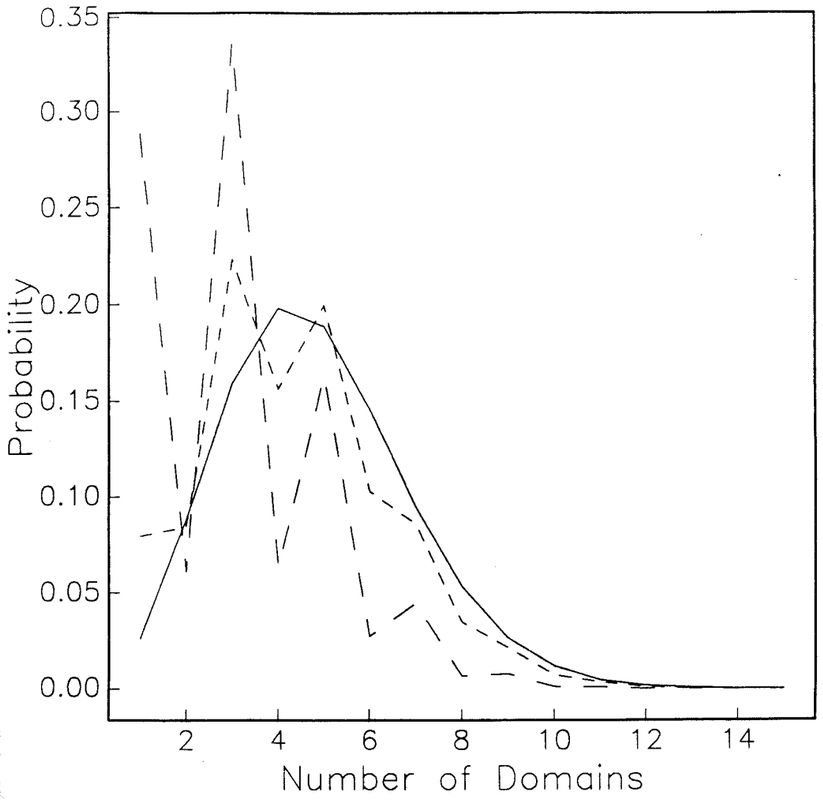

Figure 5.14 The distribution in the number of domains for 20μm grains with grid size 0.02μm and S_c=84 when a bias is considered. The solid line is for b=0; the short dashed line is for b=0.0001 (i.e. at 74.8°C); the long dashed line is for b=0.00024 (i.e. at 74°C).

field increases the probability of having an odd number of domains. The first effect is illustrated by noticing that only a single domain would be observed if the external field were sufficiently large. The second effect occurs because on the average states with an odd number of domains could carry more remanent magnetization than states with even number of domains.

Taking $74°C$ for the lowest temperature for which the model is applicable, $b = 2.4\times10^{-4}$ is an upper limit for the bias for $H = 0.42Oe$. The higher the temperature, the smaller the bias, and the less the effects of the external field have on the distribution. Therefore the curve for $b=2.4\times10^{-4}$ in figure 5.14 provides an upper limit for the effects of the field. To make a more accurate estimate of the effects of the external field, another curve with $b=1.\times10^{-4}$ (i.e. at $T=74.8°C$) is shown in figure 5.14. For this higher temperature, the distribution of number of domains is closer to the distribution with $b=0$. For comparison sake, when $T=74°C$, P_{odd} and P_{even} (the summations of probabilities of all odd number domains and even number of domains) equal 83% and 17% respectively. While for $T=74.8°C$, P_{odd} = 60% and P_{even}=40%.

According to figure 5.1, 5.2 and 5.3, an odd number of domains was observed 33 times while an even number of domains was observed 25 times (i.e. P_{odd}=57% and P_{even}=43%). Although there is a difference between the odd and even number of domains observed, the difference is not quite significant statistically. However, this small difference suggests that the cluster structure occurs very close to T_c (within $1°C$ or even $0.1°C$–$0.2°C$ below T_c). This follows since for lower temperature, the bias rate would be high enough to create much much larger differences between the odd and even number of domains.

In summary, although the external field can affect the distribution in the number of domains theoretically, the effects appear not be large enough to be easily observed when the magnitude of the field is small (e.g., in the order of the earth field). On the another hand, if

the external field is large enough, the effects of the external field on the distribution in number of domains should be observable. Then one should observe a smaller number of domains than that for H_{ex}=0 case and more incidences when an odd number of domains is observed. Of course, on occasion transdomain processes at lower temperatures can occur and when this happens the distribution will be altered. More experiments are required to test the above suggestions.

5.6 Applications

In the previous sections, renormalization group theory was used to explain the wide distribution in the number of domains for TRM. Based on the theory, the distributions in the number of domains for TRM is determined within a fraction of a degree below the Curie temperature of the material. In this section, two possible applications of the theory on rock magnetism will be discussed.

5.6.1 Transdomain Processes

Although transdomain processes are not common during experiments, they are quite possible during geological time under certain circumstances. As discussed in chapter 4, the variations in the external field, in the temperatures, and in the shape of a grain are the factors that can affect transdomain processes. The magnetic changes outside the sample can also lead to transdomain processes. For example, the macrostresses which a magnetic grain is subjected to may be variable during geological time. As we have seen the macrostresses is an important factor on magnetic anisotropy (chapter 3). Therefore a change in macrostress may cause transdomain processes. Since domain walls are believed to be pinned by defects and those defects may be mobile, transdomain processes may also be caused by the movement of defects. If transdomain processes occur, they probably result in producing

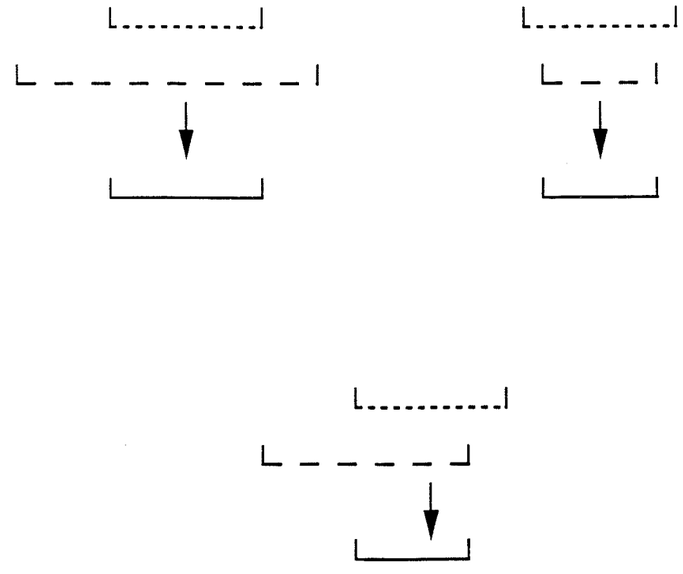

Figure 5.15 Transdomain processes change the range in the number of domains of the original TRM. The expected final range is either narrower or the same as the original range. The short dashed line gives the range in the number of domains for original TRM; the long dashed line gives the range in the number of domains for LEM states; the solid line gives the range in the number of domains after transdomain processes.

secondary remanent magnetization in the sample, e.g, secondary VRM. Reheating a sample to a higher temperature with an external field different from the original one is yet another possible mechanism leading to transdomain processes. This means that some secondary TRM could be caused by transdomain processes.

If many grains in a rock have undergone transdomain processes, the sample should not be used for investigating the paleomagnetic field. Because of this, it is desirable to determine whether the magnetic grains have undergone significant transdomain processes.

If we consider an ensemble of magnetic grains with the same size, transdomain processes will make the final range in the number of domains narrower than that original (i.e. the range for the original TRM) (figure 5.15). Therefore by observing the distribution of number of domains for same size grains, one can tell whether significant transdomain processes have happened. Experimentally, the inspection could be done by comparing the distributions of number of domains for a sample in its NRM state and after a heating cycle (heating above T_c and then cooling back to room temperature). If the range in the number of domains for the NRM state is the same as that after the heating cycle, then the sample has not undergone significant transdomain processes; in contrast, if the former is much narrower than the latter, then significant transdomain processes have occurred and the sample may not be useful for paleomagnetic studies.

5.6.2 Distinguishing Secondary Grain Growth CRM from Primary TRM

There are two main kinds of CRMs which are grain growth CRM (or authigenous) and CRM resulting from altering one magnetic mineral to another. Grain growth CRM is defined as the remanent magnetization a grain obtained during its growth in a magnetic field. Only grain growth CRM is considered here.

Consider two ensembles of grains with the same grain size, ensemble A and ensemble

B. Ensemble A is the reference ensemble and is assumed not to have changed its grain size since obtaining a primary TRM. undergone any transdomain processes. In contrast, the grains in ensemble B have acquired a grain growth CRM. Because the grains were smaller when the domain states were initially established, we would expect that the distribution in the number of domains for ensemble B is narrower than that for ensemble A. In addition, the range of domains for ensemble B should be smaller than that for ensemble A. Assuming few or no transdomain processes have occurred, we can distinguish grain growth CRM from TRM by observing the distributions in the number of domains for the two ensembles. Even if there were transdomain processes in ensemble B, a narrower range of number of domains is still expected (as discussed above). Experimentally, the distribution in the number of domains for ensemble A can be obtained by heating the sample above Curie temperature and then cooling back to room temperature within an external field roughly equal to earth field. The distribution of domains can be compared to the initial distribution observed before heating.

The above is an example of how to distinguish one form of secondary magnetization from primary magnetization. Additional work is needed to see if similar principle apply to other forms of secondary magnetizations.

5.7 Conclusions

The observational results given by Halgedahl (1991) in the distribution of number of domains for TRM in AMTM60 samples, cannot be explained by current domain theory. Investigations indicate that the relative wide ranges of number of domains observed could not be caused by low temperature transdomain processes or by the transitions between corkscrew structures. Therefore the distribution in the number of domains for TRM is believed to be determined by its initial states at temperatures within a degree below Curie

temperature of the sample. By using a renormalization, we could explain the observed distributions. Although some parameters used in the model can not be well determined at this stage, our results appear not to be significantly affected by these uncertainties.

If an external field is large enough, it should affect the distribution in the number of domains. Possible effects of an external field on the distribution in the number domains include: (1) narrower range than that for no external field; (2) a shift toward fewer number of domains; and (3) an increase in the ratio of odd number of domains than an even number of domains. Based on the observational results given by Halgedahl (1991), for AMTM60, an external field with a magnitude of the order of the earth's field does not appear to significantly affect the distribution in the number of domains. Additional data on the distribution in the number of domains for larger external field are needed.

Based on the wide range of number of domains for TRM and the fact that essentially any transdomain processes at low temperature will reduce the distribution in the number of domains relative to that of the original TRM, our theory may prove useful in paleomagnetism. In particular, by observing the distribution in the number of domains for a sample, one can: (1) determine if significant transdomain processes occurred during geological time and (2) determine whether the sample has acquired a secondary grain growth CRM since its formation.

CHAPTER 6

DISCUSSION

The conclusions of this thesis are given at the end of the individual chapters and in the abstract. Therefore the entire conclusions will not be repeated here. Instead some projects that are extensions of this thesis and which deserve further research are discussed.

The effects of macrostress on domain structures have been discussed in chapter 3. One of the major results of this work is that there appears to be a high magnitude macrostress in Ti-rich titanomagnetite samples and this macrostress reduces the number of domains. However, the origins of this stress are not clear. Probably it is caused by differences in the thermal expansion of the magnetic material and the surrounding matrix or by surface polishing. Clearly, more experimental work and some quantitative calculations are needed to test these possibilities.

The inconsistency between observation and theory for the distribution in the number of domains in magnetite has not been solved. Macrostress does not seem to play important role in the domain structures in magnetite as in titanomagnetite with large amounts of ulvospinel in solid solution. Although observational errors have been suggested as one of the possible reasons for this inconsistency, more experimental work is needed to test this possibility. Furthermore, surface structure as suggested by Ye and Merrill (1991) is also a possible cause of observational errors. This possibility needs further study.

Simple one dimensional models haven been used in chapter 4 to investigate transdomain processes. The models can be consider as a first order approximation for large grains (i.e. domain size is much large than domain wall widths, w). For small grains, especially for grains in which the domain size and w are comparable, more sophisticated models are needed for the investigation of transdomain processes.

The theory developed in chapter 4 predicts that whether interior or exterior denucleations occurs depends on the external field. Although the mechanism involved must be operating to some extent, the magnitude of the effect needs further experimental study. It is found in chapter 4 that dislocations may also affect transdomain processes. In addition dislocations can also impede walls and the first estimates of the magnitude of this effect that combine theory with domain imaging were made in chapter 4. More careful modeling and some experimental work are needed to test these ideas. Moreover, since there are interactions between defects (dislocations) and domain walls, theoretical work is needed to investigate the relationship between domain wall movement and defects movement. The theory in chapter 4 also predicts that during temperature changes, transdomain processes are unlikely for Ti-rich titanomagnetite (TM60) but are likely for Ti-poor titanomagnetite (e.g. magnetite). Obviously, more observations of domain structures for Ti-rich and Ti-poor titanomagnetite are needed.

As shown in chapter 5, for Ti-rich titanomagnetite, the distribution in the number of domains seems to be primarily determined at temperatures very close to T_c. More experimental evidence is certainly needed to support test this theory. We also need to estimate the possible observational errors (caused by surface polishing, etc.) before comparing the theory to observational results. External magnetic field may affect the distribution in the number of domain distributions as suggested in chapter 5. Domain structure observations with varying external field strength during cooling are needed.

It is suggested in chapter 5 that domain structure observations may be a good tool in distinguishing the primary TRM from secondary magnetizations. But experimental and theoretical work are needed in investigating the differences quantitatively. For example, a grain growth CRM can be modeling by considering transdomain processes as the grain grows. Mineral alteration CRM is certainly needed to be treated theoretically, since the

number of domains in an authigenically derived grain may be substantially different on the average from a diagenically altered grain.

In conclusion, some of the most important studies to be carried out in the future involve using new experiments to test some of the models given in this thesis. In addition it is important to combine theory with experiment to make rock magnetism more useful to paleomagnetists.

BIBLIOGRAPHY

Amar, H., Magnetization mechanism and domain structure of multidomain particles, *Phys. Rev., 111,* 149-153, 1958.

Appel, E., Stress anisotropy in Ti-rich titanomagnetite, *Phys. Earth Planet Inter., 46,* 233-240, 1987.

Argyle, K. S., and D. J. Dunlop, Theoretical domain pattern structure in multidomain magnetite particles, *Geophys. Res. Lett., 11,* 183-188, 1984

Banerjee, S. K., On the origin of stable remanence in pseudo-single domain grains, *J. Geomag. Geoelectr., 29,* 319-329, 1977

Bogdanov, A. A., and A. YA. Vlasov, Domain structure in a single of magnetite, *Izv. Earth. Phys. 1,* 49-58, 1965.

Bogdanov, A. A., and A. YA. Vlasov, The domain structure on magnetic particles, *Izv. Earth. Phys., 9,* 53-61, 1966.

Boyd, J., *Domain Observations on Naturally Occurring Magnetite,* Master Thesis, UC Santa Brabara, 1986.

Boyd, J. R., M. Fuller, and S. Halgedahl, Domain wall nucleation as a controlling factor in the behavior of fine magnetic particles in rocks, *Geophy. Res. Lett., 11,* 193-196, 1984.

Brown, Jr., W. F., *Micromagnetics,* 144pp, John Wiley &Sons, New York, 1963.

Bruce, A., and D. Wallace, *The New Physics,* Edited by P. Davies, 516pp, Cambridge, New York, 1989

Carmichael, R. S., Magnetic properties of minerals and rocks, in *CRC Handbook of Physical Properties of Rocks,* 345pp., CRC Press, 1982.

Chikazumi, S., *Physics of Magnetism,* p. 554, John Wiley, New York, 1964.

Dunlop, D. J., The hunting of the "Psark", *J. Geomag. Geoelectr., 29,* 293-318, 1977.

Enkin, R. J., and D. J. Dunlop, A micromagnetic study of pseudo-single domain remanence in magnetite, *J. Geophys. Res., 92,* 12726-12740, 1987.

Fletcher, E. J., and W. O'Reilly; Contribution of Fe^{2+} ions to the magnetocrystalline anisotropy constant K_1 of $Fe_{3-x}Ti_xO_4$ ($0<x<.1$), *J. Phys. C: Solid State Phys., 7,* 171-178, 1974

Fuller, M. D., Geophysical aspects of paleomagnetism, *Crit. Rev. Solid State Phys., 1,* 137-219, 1970

Halgedahl, S. L., Domain pattern observation in rock magnetism: Progress and problems, *Phys. Earth Planet. Inter., 46,* 127-163, 1987.

Halgedahl, S. L., Magnetic Domain Patterns Observed on Synthetic Ti-Rich Titanomagnetite as a Function of Temperature and in States of Thermoremanent Magnetization, *J. geophys. Res., 96,* 3943-3972, 1991.

Halgedahl, S. L., and M. Fuller, The dependence of magnetic domain structure upon magnetization state with emphasis upon nucleation as a mechanism for pseudosingle domain behavior, *J. Geophys. Res., 88,* 6505-6522, 1983

Hartmann, U., Origin of Brown's coercive paradox in perfect ferromagnetic crystals, *Phys. Rev., 36,* 2331-2332m 1987

Heider, F., S. Halgedahl and D.J. Dunlop, Temperature Dependence of Magnetic Domains in Magnetite Crystals, *Geophys. Res. Lett. 15,* 499-502, 1988.

Heider, F., and V. Hoffmann, Magneto-optical Kerr effect on magnetite crystals with externally applied magnetic fields, *Earth Planet. Sci. Lett., 108,* 131-138, 1992

Heider, F., and W. Williams, Note on temperature dependence of exchange constant in magnetite, *Geophys. Res. Lett., 15,* 184-187, 1988

Hoffmann, V., R. Schafer, E. Appel, A. Hubert, and H. Soffel, First domain observations with the magneto-optical Kerr effect on Ti-ferrites in rocks and their synthetic equivalents, *J. Magn. Magn. Mater., 71,* 90-94, 1987.

Kittel, C., Physical theory of ferromagnetic domains, *Rev. Mod. Phys., 21,* 541-583, 1949.

Landdau, L., and L. Lifshitz, On the theory of the dispersion of magnetic permeability in ferromagnetic bodies, *Phyzik Z. Sowjet., 8,* 153-169, 1935

Lilley, B. A., Energies and Widths of Domain Boundaries in Ferromagnetics, *Phyl. Mag., 41.,* 792-813, 1950.

Metcalf, M., and M. Fuller, Domain observations of titanomagnetites from room temperature to Curie point and the nature of thermoremanent magnetism in fine particles, *Nature, 321,* 847-849, 1986.

Moon, T., Trans-domain TRM, Ph.D. Thesis, University of Washington, Seattle, 1985

Moon, T. S., Domain States in Fine Particle Magnetite and Titanomagnetite, *J. Geophys. Res., 96,* 9909-9923, 1991.

Moon, T., and R.T. Merrill, The magnetic moments of non-uniformly magnetized grains, *Phys. Earth Planet. Int., 34,* 186-194, 1984

Moon, T., and R. T. Merrill, Nucleation theory and domain states in multidomain magnetic material, *Phys. Earth Planet. Int., 37,* 214-222, 1985.

Moon, T., and R. T. Merrill, Magnetic screening in multidomain material, *J. Geomagn. Gepelectr., 38,* 883-894, 1986

Morgan, G.E., and P.P.K. Simth, Transmission electron microscope and rock magnetic investigations of remanence carriers in a Precambrain metadolerite, *Earth Planet. Sci. Lett., 53,* 226-240, 1981

Morrish, A. H., *The Physical Principles of Magnetism,* 680pp, John Wiley & Sons, New York, 1965

Moskowitz, B. M., High temperature magnetostriction in magnetite and titanomagnetite, *J. Geophys. Res.,* in press, 1993.

Moskowitz, B. M. and S. L. Halgedahl, Theoretical temperature and grain size dependence of domain state in x=0.6 titanomagnetite, *J. Geophys. Res., 92,* 10,667-10,683, 1987.

Moskowitz, B. M., S. L. Halgedahl, and C. A. Lawson, Magnetic domains on unpolished and polished surfaces of titanium-rich titanomagnetite, *J. Geophys. Res., 93,* 3372-3386, 1988.

Neel, L., Theorie du trainage magnetique des ferromagnetiques en grains fins avec applications aux terres cuites, *Ann. Geophys., 5.,* 99-136, 1949.

Neel, L. Some theoretical aspects of rock magnetism, *Adv. Phys., 4,* 191-242, 1955

Newell, A. J., D. J. Dunlop, and W. Williams, A two-dimensional micromagnetic model of magnetizations and fields in magnetite, *J. Geophys. Res.,* in press, 1993.

O'Reilly, W., *Rock and Mineral Magnetism,* Blackie: Chapman and Hall, N.Y., 220pp, 1984.

Rhodes, L., and G. Rowlands, Demagnetising energies of uniformly magnetised rectangular blocks, *Proc. Leeds Philos. Lit. Soc., June,* 191-210, 1954.

Shcherbakov, V. P., S. A. Tarashtchan, and B. E. Lamash, Domain structure of PSD and MD grains and its temperature rearrangement, *Phys. Earth Planet. Inter.,* 1991

Simth, P.P.K., The application of Lorentz electron microscopy to the study of rock magnetism, *Inst. Phys. Conf. Ser. 52,* 125-128, 1980

Soffel, H., The Single-Domain-Multidomain Transition in Natural intermediate

Titanomagnetite, *Z. Geophys.,* 37, 451-470, 1971.

Soffel, H., and E. Appel, Domain structure of small synthetic titanomagnetite particles and experiments with IRM and TRM, *Phys. Earth Planet Inter., 30,* 348-355, 1982.

Soffel, H., E.R. Deutsch, E. Appel, P. Eisenach, and N. Petersen, The domain structure of synthetic stoichiometric TM10-TM75 and Al-, Mg-, and Mn- and V-doped TM62 titanomagnetite, *Phys.*Earth 336-346, 1982.

Stacey, F. D., A generalized theory of thermoremanence, covering the transition from single-domain to multidomain magnetite grains, *Philos. Mag., 7,* 1887-1900, 1962

Stacey, F. D., The physical theory of rock magnetism, *Adv. Phys., 12,* 45-133, 1963

Stacy, F. D., and S. K. Banerjee, *The Physical Principles of Rock Magnetism,* Elsevier, New York, 1974

Stapper, C. H., Micromagnetic solution for ferromagnetic sphere, *J. Appl. Phys., 40,* 798-802, 1969.

Syono, Y., Magnetocrystalline anisotropy and magnetostriction of Fe_3O_4–Fe_2TiO_4 series with special application to rock magnetism, *Jpn. J. Geophys., 4,* 71-143, 1965.

Verhoogen, J., The origin of thermoremanent magnetization, *J. Geophys. Res., 64,* 2441-2449, 1959

William, W., and D. J. Dunlop, Three-dimensional micromagnetic modeling of ferromagnetic domain structure, *Nature, 337,* 634, 1989

Worm, H.-U., P. J. Ryan and S. K. Banerjee, Domain size, Closure Domains, and the Importance of Magnetostriction in Magnetite, *Earth Planet. Sci. Lett., 102,* 71-78, 1991.

Wright, C. E., Note on the Potential and Attraction of Rectangular Bodies, *Phil. Mag., 10,* 110, 1930.

Xu, S., Microcoercivity and Bulk Coercivity in Multidomain Materials, Ph.D. Thesis, University of Washington, Seattle, 1989.

Xu, S. and R. T. Merrill, Microstress and microcoercivity in multidomain grain, *J. Geophys. Res., 94,* 10,627-10,636, 1989.

Xu, S., and R. T. Merrill, Thermal variation of domain wall thickness and number of domains in magnetic rectangular grains, *J. Geophys. Res., 95,* 21433-21440, 1990.

Ye, J., and R. T. Merrill, Differences between magnetic domain imaging observations and theory, *Geophys. Res. Lett., 18,* 593-596, 1991.

APPENDIX A

DIFFERENCES BETWEEN MAGNETIC DOMAIN IMAGING OBSERVATIONS AND THEORY

DIFFERENCES BETWEEN MAGNETIC DOMAIN IMAGING OBSERVATIONS AND THEORY

Jun Ye and Ronald T. Merrill

University of Washington, Seattle

Abstract. A quasi-two-dimensional model is developed to calculate domain structures in magnetite grains containing two to 20 domains. The calculation shows that "domains" do not consist of uniformly magnetized regions, consistent with the conclusions previously carried out on sub-micron grains, but that they become more uniformly magnetized for grains containing several domains, consistent with domain imaging results. In spite of improvement over previous calculations, there remains a significant difference between the number of domains observed and calculated.

Introduction

Domain observation [e.g., Soffel, 1971; Halgedahl and Fuller, 1983; S. Halgedahl, submitted, 1990] and theory [e.g., Moon and Merrill, 1984, 1985; Enkin and Dunlop, 1987] converged during the last decade during which it was recognized there is often more than one domain state accessible to a grain at a given temperature and pressure. Although further convergence was expected when this one-dimensional theory was extended to three dimensions, such convergence did not occur. There are at least two major differences between domain theory and observations. The first is that the calculated number of domains for a given grain is usually significantly larger than observed using Bitter patterns (e.g. S. Halgedahl, submitted, 1990) and the second is that three-dimensional numerical modeling of small magnetite grains indicates far more complex structure than expected from observation [e.g. Williams and Dunlop, 1989]. In this paper we argue that the differences between theory and observation are not as serious as sometimes perceived in the second case cited above and may partially reflect the fact that three-dimensional theory is carried out on submicron grains, whereas observations are carried out on much larger grains. Unfortunately the first problem stated above remains unsolved. During the writing of this paper one of us (R. T. M.) received for review a manuscript that arrives at similar conclusions based on three-dimensional calculations carried out on a supercomputer for submicron magnetite grains (W. Williams and D. Dunlop, submitted, 1991). In contrast, our calculations involve quasi-two-dimensional calculations for far larger grains. Neither study is definitive, but together they are persuasive that we are on the correct path to eventually reconcile theory and observation.

Paper number 91GL00817
0094-8534/91/91GL-00817$03.00

Calculation of the Magnetic Energy in Quasi-Two-Dimensional Models

The total magnetic energy E, in a magnetic grain is the sum of the exchange energy E_{ex}, the magnetocrystalline energy E_k, the magnetoelastic energy E_m, and the magnetostrictive energy. Because the latter energy depends on the type and distribution of defects, it is often ignored in domain structure calculations. This gives

$$E = E_{ex} + E_k + E_m \tag{1}$$

and a solution is sought that minimizes this energy. However, even with the use of supercomputers, three-dimensional calculations require certain additional assumptions and are presently impractical for grain sizes that are used in domain imaging techniques [e.g., Williams and Dunlop, 1989]. One result seems to be common for all previous micromagnetic calculations made on small grains: domains are not regions of uniform magnetization, and transitions to domain wall structures occur [e.g., Stapper, 1969; Moon and Merrill, 1984; Enkin and Dunlop, 1987; and Williams and Dunlop, 1989].

In the following calculations we assume that there is a surface layer in which the spin structure can differ from the underlying domain. For computational simplicity this surface layer is assumed to be uniformly thick. Although micromagnetic calculations on small grains indicate this is not the case, this assumption is an improvement over previous calculations involving larger grains, in which domains are assumed to be uniformly magnetized. The directions of the spins within the surface layer (with thickness of δ), are assumed to satisfy

$$\alpha(z) = \alpha_0 \left[1 - \frac{z}{\delta} \right] \tag{2}$$

where $\alpha(z)$ is the angle of the moment at position z and the z axis, taken to be perpendicular to the surface, and α_0 is the angle of the magnetic moments of the layer closest to the surface. The moments in the interior of the domain are along the z axis (Figure 1). For domains exhibiting the opposite magnetization it is mathematically convenient to measure α with respect to the $-z$ axis. Domain walls are assumed to be 180° Bloch walls in which the spins lie in the $y - z$ plane and are described by $\theta_z(x)$, the angle with respect to the z axis

$$\theta_z(x) = \pi \frac{x}{d_w} \tag{3}$$

where d_w is the domain wall thickness. For grains containing many domains, d_w may be approximated as a constant. These assumptions require that there is also a surface layer within the domain walls to minimize exchange energy. In this domain wall surface layer the moments

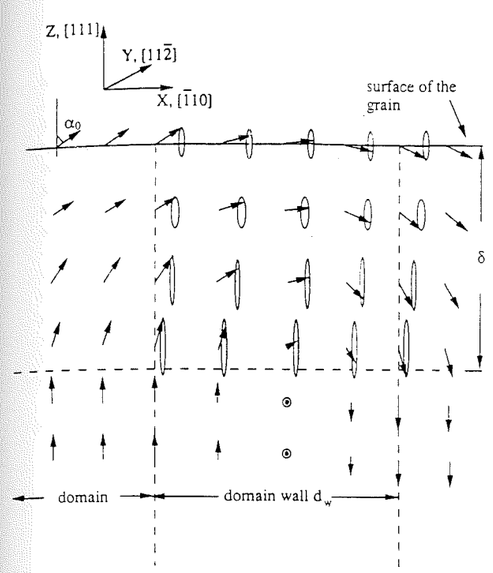

Fig. 1. The direction of magnetization within the surface layer of a domain and a domain wall. The surface layer thickness δ and the surface turning angle α_0 are the variables determined in the calculations.

are assumed to lie along a cone for a given z. The cone axis is in the x direction and the angle the moments make with respect to the x axis is taken to be

$$\theta_x(z) = \frac{\pi}{2} - \alpha(z) \tag{4}$$

Note that this implies the cone angle is a function of z. The angle of the component of the moment in the y-z plane with respect to the z axis is given by equation (3) (Figure 1). Because of the assumptions made, we refer to these calculations as a quasi-two-dimensional model.

The exchange energy is given by

$$E_{ex} = A \int_V \left[(\nabla\alpha_1)^2 + (\nabla\alpha_2)^2 + (\nabla\alpha_3)^2\right]dV \tag{5}$$

where A is the exchange constant and taken to be 1.29×10^{-11} J/m for magnetite at room temperature [Moskowitz and Halgedahl, 1987], and α_i are the direction cosines with respect to the i axis. An analytical expression for E_{ex} can be obtained for the quasi-two-dimensional model that depends on the number of domains n, the thickness of the surface layer δ, grain size D (linear dimension of cube), and α_0. (Details of calculations used in this paper but omitted for brevity's sake can be obtained from the first author.) E_{ex} is found to be

$$E_{ex} = AD\left\{2\alpha_0^2\frac{D}{\delta} + (n-1)\frac{\pi^2}{d_w}\left[D - \left[1 - \frac{\sin 2\alpha_0}{2\alpha_0}\right]\delta\right]\right\} \tag{6}$$

The magnetocrystalline anisotropy energy E_k is approximated by

$$E_k = \int_V \left[K_1(\alpha_1^2\alpha_2^2 + \alpha_1^2\alpha_3^2 + \alpha_2^2\alpha_3^2)\right]dV \tag{7}$$

where the room temperature value for magnetite's K_1 anisotropy constant is taken to be -1.36×10^4 J/m^3 [Syono, 1965]. The z axis is taken to lie along the [111] direction of magnetite, and the y axis is taken to lie along the [0$\bar{1}$1] direction. The magnetocrystalline anisotropy can also be analytically calculated for the quasi-two-dimensional model and is found to be

$$E_k = K_1 D\left[2(D-(n-1)d_w)\,\delta f_1(\alpha_0) + 2(n-1)\delta d_w\, f_2(\alpha_0) + \frac{7}{32}(n-1)(D-2\delta)d_w\right] \tag{8}$$

where $f_1(\alpha_0)$ and $f_2(\alpha_0)$ are given by

$$f_1(\alpha_0) = \frac{7}{32} + \frac{1}{\alpha_0}\left[\frac{1}{48}\sin 2\alpha_0 + \frac{7}{384}\sin 4\alpha_0 + \frac{1}{2\sqrt{18}}\sin^2\alpha_0 - \frac{1}{4\sqrt{18}}(1 - \cos^4\alpha_0 - \sin^4\alpha_0)\right] \tag{9}$$

$$f_2(\alpha_0) = \frac{53}{256} - \frac{1}{\alpha_0}\left[\frac{3}{512}\sin 2\alpha_0 + \frac{1}{16}\sin^3\alpha_0 - \frac{7}{128}\sin\alpha_0\cos^3\alpha_0 + \frac{1}{128}\sin 4\alpha_0 + \frac{2}{9\sqrt{3}\pi}(1-\cos^4\alpha_0)\right] \tag{10}$$

The first term in (8) is the magnetocrystalline energy from the surface layer in the domain, the second term is that due to the surface layer in the wall, and the last is due to the remainder of the wall.

Unlike previous one-dimensional calculations on large grains, "bound magnetic charge" now is present in the interior of the domain. The magnetostatic energy is

$$E_m = \frac{1}{2}\int_V\int_V \frac{\rho\rho'}{|\vec{r}-\vec{r}'|}dVdV' + \int_S\int_V \frac{\sigma\rho'}{|\vec{r}-\vec{r}'|}dSdV' + \frac{1}{2}\int_S\int_S \frac{\sigma\sigma'}{|\vec{r}-\vec{r}'|}dSdS' \tag{11}$$

where $\rho = -\nabla\cdot\vec{M}_s(x,y,z)$ and $\rho' = -\nabla\cdot\vec{M}_s(x',y',z')$ are the volume charge densities, $\sigma = \hat{z}\cdot\vec{M}_s(x,y,z)$ and $\sigma' = \hat{z}\cdot\vec{M}_s(x',y',z')$ are the surface charge densities with $\hat{z}$ being the unit vector in the z direction, and $\vec{M}_s$ is the magnetization of magnetite taken to be 480×10^3A/m. $\vec{r} = \vec{r}\,(x,y,z)$ and $\vec{r}\,' = \vec{r}\,'(x',y',z')$ are the positions of integral elements. V is the volume of the grain, S is its surface area, and r is the distance between the designated bound charges. To evaluate the first and second terms of (11), the surface layer was divided into a series of discrete sublayers within which the magnetization is assumed to be uniform. Convergence can be tested by repeating the calculations for an increased number of sublayers. A numerical method modified somewhat from that used by Rhodes and Rowlands [1954] was used to obtain E_m. For simplicity, we use a constant wall thickness (0.08 μm) throughout our calculation and the wall positions have been chosen to let the total energy be minimum in a given number of domains.

Results

Figure 2 shows how the reduced energy (total magnetic energy in equation (1) normalized by $2VJ_s^2$) varies as a function of α_0 for a cubic magnetite grain with linear dimension of 1 μm. The different curves are for different possible local energy minimum (LEM) states [Moon and Merrill, 1985], ranging from two-domain to ten-domain grains. The energies in the figure are chosen to be the minimum ones for different thicknesses of surface layers, and the dependences of the energy on thickness of surface layer (for $\alpha_0 = 90°$) will be discussed later. Calculations have also been carried out on a variety of grain sizes up to 10 μm (20 domains; not shown). In all cases (for any grain size and any given number of domains) $\alpha_0 = 90°$ is the minimum energy state, indicating that strictly uniformly magnetized domains of magnetite probably do not exist, even for large grains.

Figure 3 shows the relative thickness of the surface layer (the ratio of the surface layer to grain size) as a

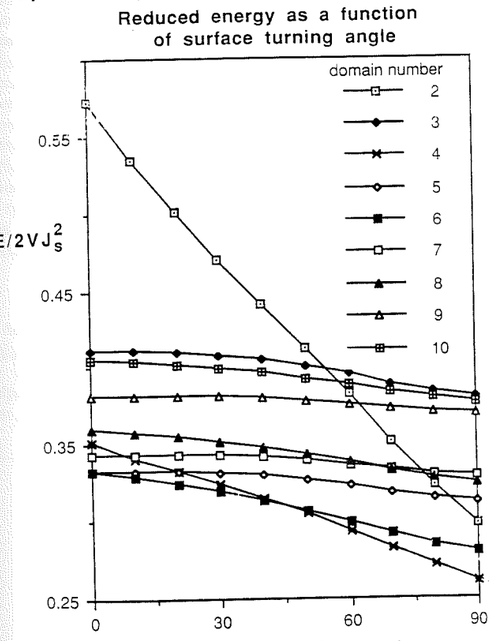

Fig. 2. The reduced energy (energy in equation 1 normalized by $2VJ_s^2$) is shown as a function of surface turning angle α_0 for 1μm grain containing from 2 to 10 domains. V is the volume of the grain, and J_s is the saturation magnetization of magnetite at room temperature (480×10^3A/m). The energies are chosen to be the minimum one for different thicknesses of surface layer. In addition E_k for an uniformly magnetized grain is set to zero because we are interest in the relative energies in this figure.

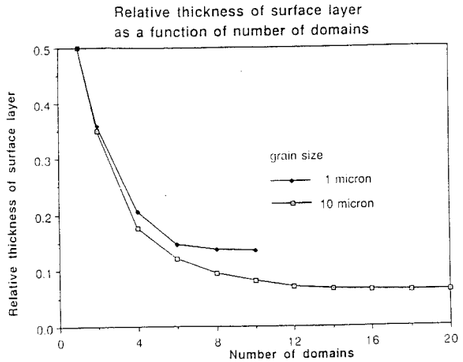

Fig. 3. Curves for the relative thickness of the surface layer versus the number of domain are given for cubic magnetite grains of 1 μm and 10 μm (linear dimension). The curve for 1 μm grain has been truncated because the grain can not contain more than 12 domains.

variation of number of domains for magnetite grains with grain sizes 1 μm and 10 μm with the surface turning angle being fixed at minimum energy state ($\alpha_0 = 90°$). This illustrates that the deviation from the classical uniformly-magnetized domain state decreases with both grain size and number of domains. That is, although there probably are not completely uniformly-magnetized domains in magnetite, the uniformly magnetized domain state may be a very good approximation in large grains.

Table 1 gives the number of domains in an absolute, or global, energy minimum (GEM) state as a function of grain size. A comparison with those found by Moon and Merrill [1985] is also given. As expected, the number of GEM states (and the range of LEM states) is shifted to fewer domains for a given grain size. Calculations for the uniform domain structure were made by choosing surface turning angle $\alpha_0 = 0$. Exchange constant A, anisotropy constant K_1, and saturation magnetization M_s are chosen for magnetite to be: $A = 1.29\times10^{-11}$J/m, $K_1 = -1.36\times10^4$J/m^3, and $M_s = 480\times10^3$A/m.

TABLE 1. The number of domains in GEM states for a given grain size.

grain size (micron)	n (uniform)	n (non-uniform)
1	5	4
2	8	6
3	9	8
4	10	8
5	12	10
6	13	10
7	14	10
8	14	12
9	15	14
10	16	14

Conclusions

The calculations given in this paper are for simplistic domain structures that model deviation from the non-uniformly magnetized state with a non-uniformly magnetized surface layer. That these structures are not completely accurate is clearly evident when one compares them to more precisely calculated structures in submicron grains [e.g., Williams and Dunlop, 1989]. Nevertheless, these structures are preferable to the uniformly-magnetized domain structures usually assumed for large grains. In particular, one can use this modeling procedure to determine changes in the complexity of domain structure as a function of grain size in large grains.

Based on three-dimensional micromagnetic calculations on submicron grains, Williams and Dunlop (submitted, 1991) have suggested that the variation in magnetic structure decreases somewhat with increase in grain size, all other factors held constant. In this paper we have reported the results from quasi-two-dimensional calculations made for cubic anisotropy "magnetite" cubes with linear dimensions that vary from 1 μm to 10 μm. Our results show that deviations from uniformly-magnetized domains probably always exist, but the deviations are small for grains containing many domains. Moreover, fewer domains are expected for a given grain volume than previously calculated. These results reduce the differences between domain imaging observation and theory. Nevertheless one outstanding difference remains: in spite of the additional magnetic structure considered in this paper, the number of domains remains significantly smaller than calculated.

Acknowledgments. Song Xu made several helpful suggestions during the early stages of this study. Reviews by Sue Halgedahl, Song Xu, and an anonymous person helped to improve this paper. Funding for this research was provided by the National Science Foundation.

References

Enkin, R. J. and D. J. Dunlop, A micromagnetic study of pseudo-single-domain remanence in magnetite, *J. Geophys. Res., 92*, 12726, 1987.

Halgedahl, S. L. and M. Fuller, The dependence of magnetic domain structure upon magnetization state with emphasis upon nucleation as a mechanism for pseudo-single domain behavior, *J. Geophys. Res., 88*, 6505, 1983.

Moon, T. S. and R. T. Merrill, The magnetic moments of non-uniformly magnetized grains, *Phys. Earth Planet. Inter., 34*, 186, 1984.

Moon, T. S. and R. T. Merrill, Nucleation theory and domain states in multidomain magnetic material, *Phys. Earth Planet. Inter., 37*, 214, 1985.

Moskowitz, B. M. and S. L. Halgedahl, Theoretical temperature and grain-size dependence of domain state in x=0.6 titanomagnetite, *J. Geophys. Res., 92*, 10667, 1987.

Rhodes, P., and G. Rowlands, Demagnetizing energies of uniformly magnetized rectangular blocks, *Proc. Leeds Philo. Liter. Soc., Soc. Sect., 6*, 191, 1954.

Soffel, H. C., The single domain-multidomain transition in intermediate titanomagnetite, *J. Geophys. Res., 37*, 451, 1971.

Stapper, C. H., Micromagnetic solution for ferromagnetic sphere, *J. Appl. Phys., 40*, 798, 1969.

Syono, Y., Magnetocrystalline anisotropy and magnetostriction of Fe_3O_4–Fe_2TiO_4 series with special application to rock magnetism, *J. Geophys. Res., 4*, 71, 1965.

Williams, W. and D. J. Dunlop, Three-dimensional micromagnetic modeling of ferromagnetic domain structure, *Nature, 337*, 634, 1989.

J. Ye and R. Merrill, Geophysics Program, AK-50, University of Washington, Seattle, WA 98195.

(Received June 6, 1990;
revised October 10, 1990;
accepted November 15, 1990.)

APPENDIX B

IMPROVED EVALUATION OF INTEGRALS RELATED TO MAGNETOSTATIC ENERGIES

The following integral is needed in the calculation of potential energy between two three dimensional rectangular bodies (uniformly charged):

$$I = \int_{-a}^{a}\int_{-a'}^{a'}\int_{-b}^{b}\int_{-b'}^{b'}\int_{-c}^{c}\int_{-c'}^{c'} \frac{dxdx'dydy'dzdz'}{[(\xi+x'-x)^2+(\eta+y'-y)^2+(\zeta+z'-z)^2]^{1/2}} \tag{B1}$$

By using :

$$\xi+x'-x = u$$

$$\eta+y'-y = v \tag{B2}$$

$$\zeta+z'-z = w$$

and

$$P^2 = u^2+v^2+w^2 \tag{B3}$$

The integral, (B1), becomes

$$I' = \iiint\iiint \frac{(du)^2(dv)^2(dw)^2}{P} \tag{B4}$$

More general, integrals like $\iint\frac{(du)^2}{P}$, $\iint\frac{dudv}{P}$, $\iiint\frac{(du)^2dv}{P}$, $\iiint\frac{dudvdw}{P}$, $\iiint\iint\frac{(du)^2(dv)^2}{P}$, $\iiint\iint\frac{(du)^2dvdw}{P}$ and $\iiint\iint\frac{(du)^2(dv)^2dw}{P}$ are needed for calculating the potential energy for one, two or three dimensional bodies. Although the formulas of these integrals were given by Wright (1930), their application produced incorrect results (Rhodes and Rowlands, 1954). The integrals are

$$\int \frac{du}{P} = log\,(u+P)+C \tag{B5}$$

$$\int \frac{(du)^2}{P} = ulog\,(u+P)-P+C \tag{B6}$$

$$\iint \frac{dudv}{P} = vlog\,(u+P)+ulog\,(v+P)+wtan^{-1}\frac{wP}{uv}+C \tag{B7}$$

$$\iiint \frac{(du)^2dv}{P} = uvlog\,(u+P)+uwtan^{-1}\frac{wP}{uv}+\frac{1}{2}(u^2-w^2)log\,(v+P)-\frac{1}{2}vP+C \tag{B8}$$

$$\iiint \frac{dudvdw}{P} = \sum_{u,v,w}\left[wvlog\,(u+P)+\frac{1}{2}u^2\tan^{-1}\frac{uP}{vw}\right]+C \tag{B9}$$

$$\iiint \frac{(du)^2(dv)^2}{P} = \frac{1}{2}u\,(v^2-w^2)log\,(u+P)+\frac{1}{2}v\,(u^2-w^2)log\,(v+P)+uvwtan^{-1}\frac{wP}{uv}+\frac{1}{2}w^2P \tag{B10}$$

$$-\frac{1}{6}P^3+C$$

$$\iiiint \frac{(du)^2dvdw}{P} = uvwlog\,(u+P)+\frac{1}{2}(u^2w-\frac{1}{6}w^3)log\,(v+P)+\frac{1}{2}(u^2v-\frac{1}{6}v^3)log\,(w+P) \tag{B11}$$

$$+\frac{1}{6}u^3\tan^{-1}\frac{uP}{wv}+\frac{1}{2}uv^2\tan^{-1}\frac{vP}{uw}+\frac{1}{2}uw^2\tan^{-1}\frac{wP}{uv}+C$$

$$\iiiint \frac{(du)^2(dv)^2dw}{P} = \frac{1}{6}uw\,(3v^2-w^2)log\,(u+P)+\frac{1}{6}vw\,(3u^2-w^2)log\,(v+P) \tag{B12}$$

$$+\frac{1}{24}(6u^2v^2-u^4-v^4)log\,(w+P)+\frac{1}{6}uv^3\tan^{-1}\frac{vP}{uw}+\frac{1}{6}uv^3\tan^{-1}\frac{uP}{vw}+\frac{1}{2}uvw^2\tan^{-1}\frac{wP}{uv}$$

$$+\frac{1}{12}Pw^3-\frac{1}{8}(u^2+v^2)Pw+C$$

$$\iiiiint \frac{(du)^2(dv)^2(dw)^2}{P} = \frac{1}{24}\sum(6u^2v^2-u^4-v^4)wlog\,(P+w)+\frac{1}{6}\sum u^3vwtan^{-1}\frac{uP}{vw} \tag{B13}$$

$$+\frac{1}{60}\sum(u^4-3u^2v^2)+C$$

The problem not seen by Wright arises from the discontinuity in the $\tan^{-1}$ term in B7 at $u=0$ and $v=0$. To avoid the discontinuity, we redefine the main value range of $\tan^{-1}$ as from 0 to π (instead of $-\frac{\pi}{2}$ to $\frac{\pi}{2}$ as previously used). The redefinition is also needed for the $\tan^{-1}$ term in B8, B9, B10, B11, B12 and B13 because they are calculated using B7.

APPENDIX C

PERMUTATION CALCULATION

The permutation of $k_2, \ldots, k_i$ which satisfy

$$m = \sum_{j=1}^{i/2}(k_{2j} - k_{2j-1}), \quad m' = \sum_{j=1}^{i/2}(k_{2j+1} - k_{2j}) \tag{C1}$$

can be calculated as follows. Define κ and κ' as

$$\kappa_j \equiv k_{2j} - k_{2j-1} \quad ; \quad \kappa'_j \equiv k_{2j-1} - k_{2j} \tag{C2}$$

The permutation of $k_2, \ldots, k_i$ satisfying (C1) equals the permutation of $\kappa_1, \ldots, \kappa_{i/2}, \kappa'_1, \ldots, \kappa'_{i/2}$ satisfying

$$m = \sum_{j=1}^{i/2}\kappa_j \tag{C3}$$

and

$$m' = \sum_{j=1}^{i/2}\kappa'_j \tag{C4}$$

Since κ and κ' are independent of each other, the permutation considered equals the product of the permutations of κs (satisfying (C3) and of κ's (satisfying (C4).

The permutation of κs satisfying (C3) is equal to the total possible ways to separate m identical members into $i/2$ groups. To calculate the permutation, let us imagine the total m members form one line. There are total $m-1$ boundaries between the members. If we choose $i/2-1$ boundaries from these $m-1$ boundaries, then the m members have been separated into $i/2$ groups. One way of separating members into $i/2$ groups corresponds to one (and only one) way of choosing $i/2-1$ boundaries. The total possible ways to choose $i/2-1$ boundaries from $m-1$ available boundaries are $C_{m-1}^{i/2-1}$, which is also equal to the permutation associated with separating m members into $i/2$ groups. Therefore the permutation

of $k_2, \ldots, k_i$ satisfying (C1) is $C_{m-1}^{i/2-1} \times C_{m'-1}^{i/2-1}$.

VITA

Jun Ye was born April 21, 1961, in Tianjin, People's Republic of China. He received his B.S. degree in Astronomy at Beijing University, Beijing, P.R.C., July 1982. In September, 1986, he received his M.S. degree in geophysics at the Graduate School of the University of Science and Technology of China, Beijing, P.R.C.